

Electrical impedance tomography with resistor networks

Liliana Borcea¹, Vladimir Druskin² and Fernando Guevara Vasquez³

¹ Computational and Applied Mathematics, MS 134, Rice University, 6100 Main St. Houston, TX 77005-1892, USA

² Schlumberger Doll Research Center, One Hampshire St., Cambridge, MA 02139-1578, USA

³ Department of Mathematics, University of Utah, 155 S 1400 E, Rm 233, Salt Lake City, UT 84112-0090, USA

E-mail: fguevara@math.utah.edu

Received 1 October 2007, in final form 12 February 2008

Published 21 April 2008

Online at stacks.iop.org/IP/24/035013

Abstract

We introduce a novel inversion algorithm for electrical impedance tomography in two dimensions, based on a model reduction approach. The reduced models are resistor networks that arise in five point stencil discretizations of the elliptic partial differential equation satisfied by the electric potential, on adaptive grids that are computed as part of the problem. We prove the unique solvability of the model reduction problem for a broad class of measurements of the Dirichlet-to-Neumann map. The size of the networks is limited by the precision of the measurements. The resulting grids are naturally refined near the boundary, where we measure and expect better resolution of the images. To determine the unknown conductivity, we use the resistor networks to define a nonlinear mapping of the data that behaves as an approximate inverse of the forward map. Then we formulate an efficient Newton-type iteration for finding the conductivity, using this map. We also show how to incorporate *a priori* information about the conductivity in the inversion scheme.

1. Introduction

In electrical impedance tomography (EIT) we wish to determine the conductivity σ inside a bounded, simply connected domain Ω , from simultaneous measurements of currents and voltages at the boundary $\partial\Omega$ [6]. Equivalently, we measure the Dirichlet-to-Neumann (DtN) map. This problem is known to be uniquely solvable given complete knowledge of the DtN map [3, 14, 28, 36, 40, 45, 46]. However, it is exponentially ill-posed [1, 39], so numerical inversion methods require regularization [29]. Because noise in the measurements limits severely the number of parameters that we can determine, we use a regularization approach based on sparse parametrizations of σ .

Regularization by means of sparse representations of the unknown in some preassigned basis of functions has been proposed for linear inverse problems in [22]. There remain at least two important questions: (1) how to design fast and efficient inversion algorithms for the nonlinear EIT problem? (2) How to choose a good basis of functions, especially when we do not have *a priori* information about σ ?

We look at bases that consist of approximate characteristic functions of cells in grids partitioning the domain Ω . The size of these grids is limited by the precision of the measurements and the location of the grid points is determined adaptively as part of the inverse problem. Here the adaptivity is with respect to the boundary measurements and not the conductivity function σ , which is the unknown. The resulting grids capture the expected gradual loss of resolution of the images as we move away from the boundary. They are refined near $\partial\Omega$ and coarse deep inside the domain.

The first adaptive grids for EIT are due to Isaacson [30, 34] (see also [15, 44]). They are based on the concept of *distinguishable* perturbations of the conductivity that give distinguishable (above the noise level) perturbations of the boundary data. The grids are built in a disc-shaped domain Ω , one layer at a time, by finding the smallest circular inclusion of radius r_n , concentric with Ω , that is distinguishable with the n th Fourier mode current excitation $\exp(in\theta)$, for $n = 1, 2, \dots$ and $\theta \in [0, 2\pi)$. The first mode penetrates the deepest in the domain and the more oscillatory modes see shallower depths in Ω . The resulting grids are refined near $\partial\Omega$, as expected. Note that they are constructed with a linearization approach that estimates the depth penetration of each Fourier mode with one inclusion at a time. However, the EIT problem is nonlinear and the accuracy of such linearization is not understood.

MacMillan *et al* [38] study distinguishability by deriving lower and upper bounds of the perturbations of the Neumann-to-Dirichlet map, in terms of a local norm of perturbations $\delta\sigma$. They use these bounds to describe approximately the set of distinguishable $\delta\sigma$ and to construct the distinguishability grids. The grids are still based on a linearization approach, with each cell determined by the smallest distinguishable inclusion at a given depth in Ω . The numerical inversion in [38] does not use the grids explicitly, but it incorporates the loss of resolution quantified by them, through weights in the objective function that they optimize to find σ .

Other resolution and distinguishability studies for EIT are given in [2, 25, 42]. They are all based on the linearization approximation. A different, nonlinear, adaptive parametrization approach is due to Ben Ameer *et al* [4, 5]. It considers piecewise constant conductivities on subsets (zones) of a two-dimensional domain discretized with some grid. The adaptivity of the parametrization consists in the iterative coarsening or refinement of the zonation, using the gradient of a least squares data misfit functional. This functional is minimized for each update of the zonation and the approach can become computationally costly if many updates of the conductivity are required.

In this paper we consider the EIT problem in two dimensions, in a disc-shaped domain Ω , and we image on adaptive grids computed with a model reduction approach. The reduced models are resistor networks of a certain topology that can predict the boundary measurements. Resistor networks have been considered in other studies of EIT. For example, they are used in [7, 8] for imaging high-contrast conductivities of a certain class, where the Dirichlet-to-Neumann map degenerates to that of a resistor network, due to strong flow channeling. Here we look at lower contrasts in the conductivity, where the networks arise from the discretization of the elliptic partial differential equation for the electric potential. This was done before, for example in [24], but the networks considered there are not uniquely recoverable from the data, because they are large and contain redundant connections.

We look at uniquely recoverable resistor networks that we can specify precisely using the foundational work [17, 18, 20, 32, 33] on circular planar graphs. The networks arise from

five point stencil discretization schemes, on adaptive grids that are computed as part of the problem. We estimate σ with a nonlinear optimization process consisting of two steps: first, we use the networks and the grids to define a nonlinear mapping of the data to the space of conductivities. This is an approximate inverse of the forward map. Then, we estimate the conductivity with a Newton-type iteration formulated for the composition of the two maps, which are approximate inverses of each other. This preconditions the iterative process and gives fast convergence.

The paper is organized as follows: we begin with the mathematical formulation of the problem in section 2. Then we state the model reduction problem in terms of resistor networks in section 3. The unique solvability of the model reduction problem is discussed in section 4. The iteration for finding σ from the resistor networks is given in section 5. The numerical results are shown in section 6. All the results are with no prior information about the conductivity. However, we show in section 7 how to incorporate such information in the imaging process. We end with a brief summary in section 8.

2. Formulation of the inverse problem

We consider the EIT problem in two dimensions, in a unit disc Ω . In principle, this extends to other simply connected domains in \mathbb{R}^2 that can be mapped conformally to the disc, but we do not address this here. We let $\sigma(\mathbf{x})$ be a positive and bounded electrical conductivity function defined in $\overline{\Omega}$ and denote by $u(\mathbf{x})$ the electric potential. It satisfies the elliptic second-order partial differential equation

$$\nabla \cdot [\sigma(\mathbf{x}) \nabla u(\mathbf{x})] = 0, \quad \mathbf{x} \in \Omega, \quad (1)$$

with Dirichlet boundary conditions

$$u(\mathbf{x})|_{\partial\Omega} = V(\mathbf{x}), \quad (2)$$

for given $V \in H^{1/2}(\partial\Omega)$. The inverse problem is to find $\sigma(\mathbf{x})$ from the DtN map

$$\Lambda_\sigma^{\text{DtN}} : H^{1/2}(\partial\Omega) \rightarrow H^{-1/2}(\partial\Omega), \quad \Lambda_\sigma^{\text{DtN}} V = \mathbf{n} \cdot (\sigma \nabla u)|_{\partial\Omega}, \quad (3)$$

where $\mathbf{n}(\mathbf{x})$ is the outward unit normal at $\mathbf{x} \in \partial\Omega$.

In practice, we typically measure the Neumann-to-Dirichlet (NtD) map

$$\Lambda_\sigma^{\text{NtD}} : H^{-1/2}(\partial\Omega) \rightarrow H^{1/2}(\partial\Omega), \quad \Lambda_\sigma^{\text{NtD}} I = u|_{\partial\Omega}, \quad (4)$$

which is smoothing and deals better with noise. This map takes boundary current fluxes

$$I = \mathbf{n} \cdot (\sigma \nabla u)|_{\partial\Omega}, \quad (5)$$

satisfying

$$\int_{\partial\Omega} I(\mathbf{x}) \, dx = 0,$$

to boundary voltages $u|_{\partial\Omega}$. Here $u(\mathbf{x})$ solves equation (1) with Neumann boundary conditions (5), and it is defined up to an additive (grounding potential) constant.

In the analysis of this paper it is convenient to work with the DtN map. It may be obtained from the measured NtD map using convex duality, as shown in appendix A.

3. Formulation of the model reduction problem

In the first step of our inversion method, we seek a reduced model for problems (1) and (2) that reproduces discrete measurements of the DtN map. We consider a particular class of measurements described in section 3.1. The reduced model is a resistor network that arises in a five point stencil discretization of equation (1), on a grid that is to be computed as part of the problem. This is shown in section 3.2.

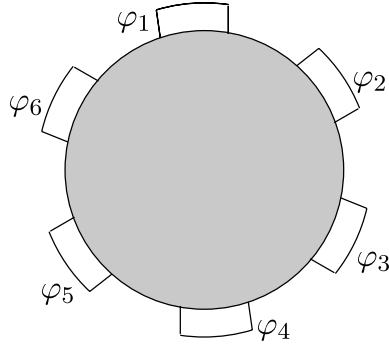


Figure 1. $\mathcal{M}_n(\Lambda_\sigma^{\text{DtN}})$ can be interpreted as measurements taken with electrodes at the boundary.

3.1. The measured DtN map

We begin the formulation of the model reduction problem with the definition of the discrete measurements of the DtN map that are to be reproduced by the reduced model. In principle, we could work with pointwise measurements of $\Lambda_\sigma^{\text{DtN}}$, as is done in [19, 20, 33]. Here we consider a more general class of measurement operators, which allow for lumping of the data at a few n boundary points. This can be useful in practice for filtering out uncorrelated instrument noise.

Definition 1 (Discrete measurements of the DtN map). *Let $\varphi_1, \dots, \varphi_n$ be a set of n nonnegative functions in $H^{1/2}(\partial\Omega)$, with disjoint supports and numbered in circular order around the boundary. They are normalized by*

$$\int_{\partial\Omega} \varphi_i(\mathbf{x}) \, d\mathbf{x} = 1, \quad i = 1, 2, \dots, n. \quad (6)$$

We define the $n \times n$ discrete measurement operator (matrix) $\mathcal{M}_n(\Lambda_\sigma^{\text{DtN}})$ with entries

$$(\mathcal{M}_n(\Lambda_\sigma^{\text{DtN}}))_{i,j} = \begin{cases} \langle \varphi_i, \Lambda_\sigma^{\text{DtN}} \varphi_j \rangle & \text{if } i \neq j, \\ - \sum_{p=1, p \neq i}^n \langle \varphi_i, \Lambda_\sigma^{\text{DtN}} \varphi_p \rangle & \text{otherwise,} \end{cases} \quad (7)$$

where $\langle \cdot, \cdot \rangle$ is the $H^{1/2}(\partial\Omega)$, $H^{-1/2}(\partial\Omega)$ duality pairing. Note that $\mathcal{M}_n(\Lambda_\sigma^{\text{DtN}})$ is symmetric and it satisfies the current conservation law

$$\sum_{i=1}^n (\mathcal{M}_n(\Lambda_\sigma^{\text{DtN}}))_{i,j} = 0, \quad j = 1, \dots, n. \quad (8)$$

Definition 1 is stated for arbitrary nonnegative functions φ_i in the trace space $H^{1/2}(\partial\Omega)$. If for example we take φ_i as indicator functions of arcs at $\partial\Omega$ (figure 1), the measurements $\mathcal{M}_n(\Lambda_\sigma^{\text{DtN}})$ correspond to the ‘shunt electrode model’ [43], with electrodes idealized as perfect conductors⁴. In this model, the potential is constant over the support of the electrodes and

$$(\mathcal{M}_n(\Lambda_\sigma^{\text{DtN}}))_{i,j} = \langle \varphi_i, \Lambda_\sigma^{\text{DtN}} \varphi_j \rangle$$

⁴ Other more accurate models such as the ‘complete electrode model’ can in principle be incorporated to the approach presented here. From the theoretical point of view this would involve proving a consistency result analogous to theorem 1 with a different electrode model. Once consistency is established, optimization could be used to find the resistors fitting the data.

is the current flowing out of electrode i , when we set the potential to φ_j at the j th electrode. This is for $i \neq j$. The diagonal entries are defined in (7) to satisfy the conservation of currents law (8).

In our implementation φ_i are not indicator functions of electrodes. They are smooth functions that we use for lumping the data at n equidistant boundary points

$$\mathbf{x}_i = (1, ih_\theta), \quad i = 1, 2, \dots, n, \quad h_\theta = \frac{2\pi}{n}. \quad (9)$$

The assumption is that we are given the potential and currents at many ($N > n$) points around the boundary. Since in practice, the high-frequency components of the data are basically noise, we filter them out by lumping at the $n < N$ points (9) on $\partial\Omega$. The details are given in section 4.3. The lumping functions are obtained by translating around $\partial\Omega$ a smooth $\varphi(\mathbf{x})$ defined in appendix B.2

$$\varphi_i = \varphi(\mathbf{x} - \mathbf{x}_i), \quad i = 1, 2, \dots, n. \quad (10)$$

We observed numerically that our algorithm does not depend on the choice of the lumping function.

Remark 1. In the remainder of the paper, we use a slight abuse of notation and let $\Lambda_\sigma^{\text{DtN}}$ be the $N \times N$ matrix of actual measurements of the DtN map. These can be pointwise measurements or measurements done at electrodes, using the shunt model (7). The lumping of these measurements at the n boundary points (9) is given by the $n \times n$ matrix $\mathcal{M}_n(\Lambda_\sigma^{\text{DtN}})$. In this case, a characterization analogous to theorem 1 holds when we do lumping of measurements, as is shown in [31, B.4].

3.2. The reduced models

Our reduced models are resistor networks that are determined uniquely by the measurements $\mathcal{M}_n(\Lambda_\sigma^{\text{DtN}})$ of the DtN map. We show this in section 4. Here we interpret the resistor networks in the context of discretizing equation (1) with a five point stencil, finite volumes scheme. We use such a scheme because it leads to critical networks (with no redundant connections) that are uniquely determined by the measurements. The interpretation of the resistor networks given below is used later, in section 5, to define a preconditioned Newton-type iteration for estimating the conductivity.

3.2.1. The staggered finite volumes grids. We discretize on staggered, primary and dual grids given by tensor products of a uniform angular grid and an adaptive, not known *a priori* radial grid. We take n equidistant primary points (9) at $\partial\Omega$, where we lump the measurements in $\mathcal{M}_n(\Lambda_\sigma^{\text{DtN}})$. This defines the uniform angle spacing⁵. The dual grid angles are the bisectors of the primary grid angles, as shown in figure 2. The potential is discretized on the primary grid points and the current fluxes on the dual grid edges.

We denote by r_i the primary radii and by \hat{r}_i the dual ones, for $i \geq 1$. The counting of the primary radii begins from the boundary,

$$0 \leq r_{\lceil l/2 \rceil + 1} < r_{\lceil l/2 \rceil} < \dots < r_2 < r_1 = 1,$$

where $\lceil l/2 \rceil$ is the smallest integer larger or equal to $l/2$. Similarly, the dual radii are counted as

$$0 < \hat{r}_{\lceil l/2 \rceil + 1} < \hat{r}_{\lceil l/2 \rceil} < \dots < \hat{r}_2 < \hat{r}_1 = 1,$$

⁵ We consider uniform angle discretizations because we assume that we have measurements all around $\partial\Omega$ and we are interested in capturing the first n Fourier modes of the boundary data. In the case of partial measurements restricted to a sector of $\partial\Omega$, the grids will be nonuniform in angle. Inversion with such data is currently under investigation.

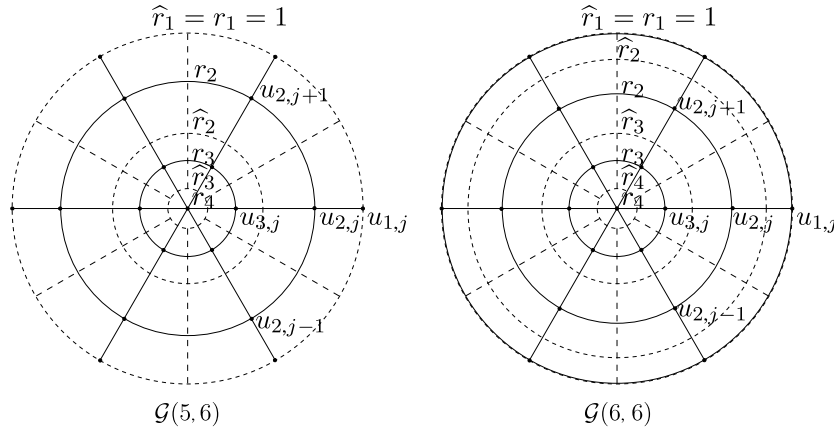


Figure 2. Examples of the two kinds of grids used. The primary grid is in solid line and the dual grid is in dotted line.

where $\lfloor l/2 \rfloor$ is the largest integer smaller or equal to $l/2$. The integer l corresponds to the number of interior grid layers or, equivalently, the number of primary and dual radii that are strictly less than 1.

We denote in short the grid by $\mathcal{G}(l, n)$. The first primary and dual radii in it coincide ($r_1 = \hat{r}_1 = 1$), in order to compute both the potential and the current flux at $\partial\Omega$. The type of the next layer depends on the parity of l . It is a primary one if l is odd and dual otherwise. We illustrate our notation in figure 2, where we show two grids with $n = 6$ primary boundary points. In the left picture we have $l = 5$ layers, corresponding to the primary and dual radii $0 \leq r_4 < \hat{r}_3 < r_3 < \hat{r}_2 < r_2 < 1$. We do not count r_1 and \hat{r}_1 because they are fixed at the boundary. In the right picture in figure 2 we have $l = 6$ layers, corresponding to $0 \leq r_4 < \hat{r}_4 < r_3 < \hat{r}_3 < r_2 < \hat{r}_2 < 1$.

3.2.2. The finite volumes scheme. We integrate equation (1) over the dual cells, and then use the divergence theorem to derive the balance of fluxes through the dual cell boundaries. These fluxes are approximated with finite differences, and the discrete equations become like Kirchhoff's node law for a resistor network with topology given by the primary grid. For details of the discretization scheme see [31, section 3.1.2].

Let $u_{i,j}$ be the approximation of potential u at the primary grid nodes (r_i, jh_θ) , for $1 \leq i \leq \lfloor l/2 \rfloor + 1$ and $1 \leq j \leq n$. Let also I_j be the approximation of the current density $I = \sigma \mathbf{n} \cdot \nabla u|_{\partial\Omega}$ at boundary point $(1, jh_\theta)$, for $1 \leq j \leq n$. We now write the discretization scheme, using the resistors

$$R_{i,j} = \int_{r_{i+1}}^{r_i} dr \left(r \int_{(j-1/2)h_\theta}^{(j+1/2)h_\theta} d\theta \sigma(r, \theta) \right)^{-1} = \frac{1}{\hat{\sigma}_{i,j}} \frac{1}{h_\theta} \int_{r_{i+1}}^{r_i} \frac{dr}{r} = \frac{\ln(r_i/r_{i+1})}{\hat{\sigma}_{i,j} h_\theta}, \quad (11)$$

for $i = 1, \dots, \lfloor l/2 \rfloor$, $j = 1, \dots, n$ and

$$\begin{aligned} \hat{R}_{i,j+1/2} &= \int_{jh_\theta}^{(j+1)h_\theta} d\theta \left(\int_{\hat{r}_i}^{\hat{r}_{i-1}} \frac{dr \sigma(r, \theta)}{r} \right)^{-1} \approx h_\theta^2 \left(\int_{\hat{r}_i}^{\hat{r}_{i-1}} dr \int_{jh_\theta}^{(j+1)h_\theta} d\theta \frac{\sigma(r, \theta)}{r} \right)^{-1} \\ &= \frac{1}{\sigma_{i,j+1/2}} h_\theta \left(\int_{\hat{r}_i}^{\hat{r}_{i-1}} \frac{dr}{r} \right)^{-1} = \frac{h_\theta}{\sigma_{i,j+1/2} \ln(\hat{r}_{i-1}/\hat{r}_i)}, \end{aligned} \quad (12)$$

for $i = 2, \dots, \lfloor l/2 \rfloor + 1$, $j = 1, \dots, n$. The coefficients $\widehat{\sigma}_{i,j}$ and $\sigma_{i,j+1/2}$ are averages of the conductivity on the grid.

At the dual cells containing primary grid nodes (r_i, jh_θ) that are neither on the boundary nor at the origin (i.e., for $2 \leq i \leq \lfloor l/2 \rfloor$ and $1 \leq j \leq n$), we have

$$\frac{u_{i-1,j} - u_{i,j}}{R_{i-1,j}} + \frac{u_{i+1,j} - u_{i,j}}{R_{i,j}} + \frac{u_{i,j+1} - u_{i,j}}{\widehat{R}_{i,j+1/2}} + \frac{u_{i,j-1} - u_{i,j}}{\widehat{R}_{i,j-1/2}} = 0, \quad (13)$$

where the operations $(+)$ and $(-)$ on the angular index j are to be understood modulo n . The cell containing the origin is a special case, as involves only radial primary layers, and the discretization is

$$\sum_{j=1}^n \frac{u_{\lfloor l/2 \rfloor, j} - u_{\lfloor l/2 \rfloor + 1, j}}{R_{\lfloor l/2 \rfloor, j}} = 0. \quad (14)$$

It remains to define the stencil for the boundary nodes. When l is odd (see figure 2 on the left), the stencil is

$$\frac{u_{2,j} - u_{1,j}}{R_{1,j}} + I_j = 0, \quad \text{for } 1 \leq j \leq n. \quad (15)$$

Otherwise, we take (see figure 2 on the right)

$$\frac{u_{2,j} - u_{1,j}}{R_{1,j}} + \frac{u_{1,j+1} - u_{1,j}}{\widehat{R}_{1,j+1/2}} + \frac{u_{1,j-1} - u_{1,j}}{\widehat{R}_{1,j-1/2}} + I_j = 0, \quad \text{for } 1 \leq j \leq n. \quad (16)$$

3.2.3. The resistor network. The discrete equations (13)–(16) are Kirchhoff's node law for a circular resistor network. We denote this network by $C(l, n)$. Its topology is determined by the primary grid in $\mathcal{G}(l, n)$ and the edges have resistors $R_{i,j}$, for $i = 1, \dots, \lfloor l/2 \rfloor$ and $\widehat{R}_{i,j+1/2}$, for $i = 2, \dots, \lfloor l/2 \rfloor + 1$ and $j = 1, \dots, n$.

Problem 1 (Model reduction). Determine the resistor network $C(l, n)$ that has as DtN map the measurements $\mathcal{M}_n(\Lambda_\sigma^{\text{DtN}})$.

We prove in section 4 that problem 1 can be solved uniquely, if the number n of boundary points is odd and the number of layers is $l = (n - 1)/2$. Note that under this restriction we have $n(n - 1)/2$ resistors in $C(l, n)$ and that this is precisely the number of independent entries in the matrix of measurements $\mathcal{M}_n(\Lambda_\sigma^{\text{DtN}})$. Because $\mathcal{M}_n(\Lambda_\sigma^{\text{DtN}})$ is symmetric and its rows sum to zero, it is completely determined by the $n(n - 1)/2$ entries in its strictly upper triangular part. The resulting network $C(l, n)$ is our reduced model that matches *exactly* the data.

3.3. The adaptive grid

According to equations (11) and (12), the resistors in $C(l, n)$ are determined by averages of $\sigma(r, \theta)$ in the grid cells. This suggests that if we knew $\sigma(r, \theta)$ we could find the grid $\mathcal{G}(l, n)$ from the resistors. However, we restrict $\mathcal{G}(l, n)$ to the class of tensor product grids and such a computation may not be possible for general two-dimensional $\sigma(r, \theta)$. In layered media with conductivity $\sigma(r)$, the network is rotation invariant

$$\begin{aligned} R_{i,j} &= \frac{1}{h_\theta} \int_{r_{i+1}}^{r_i} \frac{dt}{t\sigma(t)} = R_i, & i &= 1, \dots, \lfloor l/2 \rfloor, \\ \widehat{R}_{i,j+1/2} &= h_\theta \left(\int_{\widehat{r}_i}^{\widehat{r}_{i-1}} \frac{dt\sigma(t)}{t} \right)^{-1} = \widehat{R}_i, & i &= 2, \dots, \lfloor l/2 \rfloor + 1. \end{aligned} \quad (17)$$

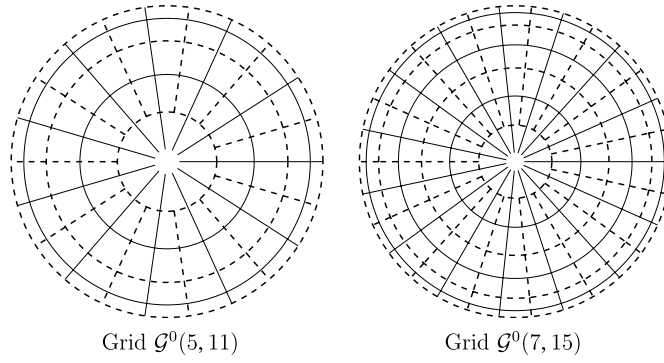


Figure 3. Grids for $\sigma^0 = 1$ (primary grid is in solid line and the dual grid is in dotted line).

Then, the computation of the primary and dual radii from the resistors is straightforward. For two-dimensional conductivities $\sigma(r, \theta)$ the resistors depend on the angular index j , for $j = 1, \dots, n$, and there is no guarantee that we can find an exact tensor product grid from the resistors. Nevertheless, the network $C(l, n)$ is unambiguously defined by the data $\mathcal{M}_n(\Lambda_{\sigma}^{\text{DtN}})$ for any $\sigma(r, \theta)$, and we can formulate a nonlinear optimization problem for estimating $\sigma(r, \theta)$, using an approximate grid. The key point of this paper is that for a class of sufficiently smooth or piecewise smooth $\sigma(r, \theta)$, we can use the grid $\mathcal{G}^0(l, n)$ corresponding to the uniform conductivity $\sigma^0 = 1$.

For $\sigma = \sigma^0 = 1$, the resistors are

$$\begin{aligned} R_{i,j}^0 &= \frac{1}{h_{\theta}} \int_{r_{i+1}^0}^{r_i^0} \frac{dt}{t} = \frac{\ln(r_i^0/r_{i+1}^0)}{h_{\theta}} = R_i^0, & i = 1, \dots, \lfloor l/2 \rfloor, \\ \widehat{R}_{i,j+1/2}^0 &= h_{\theta} \left(\int_{\widehat{r}_i^0}^{\widehat{r}_{i-1}^0} \frac{dt}{t} \right)^{-1} = \frac{h_{\theta}}{\ln(\widehat{r}_{i-1}^0/\widehat{r}_i^0)} = \widehat{R}_i^0, & i = 2, \dots, \lfloor l/2 \rfloor + 1, \end{aligned} \quad (18)$$

for $j = 1, \dots, n$, n odd and $l = (n - 1)/2$. We denote the grid by $\mathcal{G}^0(l, n)$ and obtain from (18) its primary and dual radii

$$\begin{aligned} r_1^0 &= \widehat{r}_1^0 = 1, \\ r_{i+1}^0 &= \exp(-h_{\theta}(R_1^0 + \dots + R_i^0)), & \text{for } i = 1, \dots, \lfloor l/2 \rfloor, \\ \widehat{r}_i^0 &= \exp(-h_{\theta}((\widehat{R}_2^0)^{-1} + \dots + (\widehat{R}_i^0)^{-1})), & \text{for } i = 2, \dots, \lfloor l/2 \rfloor + 1. \end{aligned} \quad (19)$$

We plot $\mathcal{G}^0(l, n)$ in figure 3, for $n = 11$ and $n = 15$. We observe the expected interlacing of the primary and dual grids, the refinement near the boundary and the coarsening inside the domain. Note that although the resistor network $C(l, n)$ has the innermost branches electrically connected, in the grid, the last layer $r_{\lfloor l/2 \rfloor + 1}$ is not at the origin. We have $r_{\lfloor l/2 \rfloor + 1} \rightarrow 0$ as $l \rightarrow \infty$ [9, 10], but we do not approach this limit here, because the size of the grid is limited severely in the presence of noise, as explained in section 4.3. For finite l , we get $r_{\lfloor l/2 \rfloor + 1} > 0$, as if we truncated the domain close to the origin, due to a finite depth penetration of electric currents.

We call $\mathcal{G}^0(l, n)$ an ‘optimal grid’ because, by construction, the discrete solution computed on it matches *exactly* the entries in $\mathcal{M}_n(\Lambda_{\sigma^0}^{\text{DtN}})$. Naturally, in the case of a variable conductivity $\sigma(r, \theta)$, the discretization on $\mathcal{G}^0(l, n)$ does not give an exact match of the data $\mathcal{M}_n(\Lambda_{\sigma}^{\text{DtN}})$. However, the discretization error is small [9], at least for a class of sufficiently smooth, or

piecewise smooth conductivities. This interpolation property of the grid $\mathcal{G}^0(l, n)$ plays a key role in our inversion algorithm, as explained in section 5.

4. The inverse problem for the resistor network

In this section we study problem 1. We prove its solvability in section 4.1 and we explain in section 4.2 how to find the network from the data $\mathcal{M}_n(\Lambda_\sigma^{\text{DtN}})$. We end in section 4.3 with a discussion of network size limitations due to noisy measurements.

4.1. Solvability of the model reduction problem

To prove the solvability of the model reduction problem, we must establish two things: (1) the consistency of the measurements with the resistor network model and (2) that $C(l, n)$ is determined uniquely by the measurements. We begin with the consistency.

Theorem 1. *For a smooth enough, positive and bounded σ , the measurement matrix $\mathcal{M}_n(\Lambda_\sigma^{\text{DtN}})$ is the DtN map of a well-connected planar resistor network.*

Let $\mathbf{x}_i, i = 1, \dots, n$ be the boundary nodes of a planar network, embedded on a circle and consecutively numbered there. The DtN map of the network is an $n \times n$ matrix, with the (i, j) entry given by the current flowing out of node \mathbf{x}_i , when the boundary potential is one at \mathbf{x}_j and zero elsewhere. The network is called well connected if any two sets of k boundary nodes, belonging to disjoint arcs of the circle, are connected by k disjoint paths in the network [17, 20].

The proof of theorem 1 is in appendix C. It is based on two results: (1) theorem 3, which is a novel characterization of the DtN map of planar regions, equivalent to that of Ingerman and Morrow [32], but involving the measurement functions (7) instead of pointwise measurements and (2) the complete characterization of the DtN maps of well-connected, circular resistor networks from [18, 20].

The following lemma from [18, 20] defines the class of networks that can be uniquely recovered from their DtN map.

Lemma 1. *A resistor network is said to be recoverable when its resistors can be uniquely determined from the DtN map. A network is recoverable if and only if it is critical. This means that the network is well connected and the removal of any edge makes the network not well connected.*

The unique solvability of the model reduction problem is given by the next theorem.

Theorem 2. *The networks $C(l, n)$ are uniquely recoverable from their DtN map if and only if n is odd and $l = (n - 1)/2$.*

Proof. That $C((n - 1)/2, n)$ is critical and therefore recoverable for $n = \text{odd}$ follows from proposition 2.3 and corollary 9.4 in [21]. Let us show then that there is no critical network $C(l, n)$ for $n = \text{even}$.

A critical network with n boundary nodes has $n(n - 1)/2$ edges (see [20, section 5]). This is the same as the number of independent entries in the DtN map. If n is even, the number of edges in a critical network with n boundary nodes is $n(n - 1)/2 \equiv n/2 \pmod{n}$. However, the number of edges in $C(l, n)$ is $nl \equiv 0 \pmod{n}$. Therefore $C(l, n)$ is not a critical network when n is even. \square

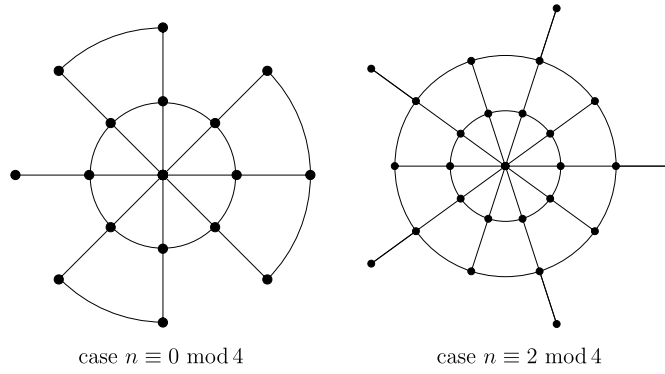


Figure 4. Critical networks for an even number n of boundary points. The construction is slightly different depending on $n \pmod{4}$ (taken from [21, pp 20–24]).

It is possible to construct critical networks with an even number of boundary nodes (see figure 4), but their topology is fundamentally different from that of $C(l, n)$.

4.2. Finding the resistor network from the measurements

To recover the critical resistor network $C(l, n)$ from the data, we use the algorithm introduced by Curtis *et al* [19]. This determines the resistors layer by layer, starting from the boundary of the network. This algorithm is fast and simple to implement, but it becomes unstable for large networks. We observed a typical loss of precision in the resistors of a factor of ten, when going from one layer to the next. In the presence of noise, we regularize the problem by keeping the network small, as we see next. This is what allows us to use the layer peeling Curtis *et al* [19] algorithm.

Remark 2. An alternative way of finding the network $C(l, n)$ from the measurements $\mathcal{M}_n(\Lambda_\sigma^{\text{DtN}})$ is to solve a nonlinear, least squares optimization problem. This has been done recently in [11]. It is observed that the optimization algorithm produces the same results as the layer peeling one, for small n . For larger n , the layer peeling algorithm breaks down, as produces negative resistors. The optimization method is slightly more robust but it breaks down as well, as n increases. The threshold n over which these methods become unstable depends on the noise level.

4.3. The resistor network for noisy measurements

We regularize problem 1 by restricting the network $C(l, n)$ size with a criterion based on the precision of the measurements. This can be done in at least two ways.

Method 1. Consider a sequence of problems, for $n_k = 2k + 1$ boundary points at which we lump the data into the matrix $\mathcal{M}_{n_k}(\Lambda_\sigma^{\text{DtN}})$, using the lumping functions (10). Here $k \geq 1$ and we note that the smaller the k is, the more smoothing or noise filtering we do on the data. For each n_k we determine the resistor network $C((n_k - 1)/2, n_k)$ from $\mathcal{M}_{n_k}(\Lambda_\sigma^{\text{DtN}})$, as explained in section 4.2. We define the threshold n as the largest n_k for which we obtain a network with

positive resistors and we keep the corresponding network $C((n-1)/2, n)$ as our reduced model.

Method 2. An alternative way of estimating the threshold n is given by the distinguishability ideas of Isaacson [34] (see also [16]). This involves the singular value decomposition of $\Lambda_\sigma^{\text{DtN}} - \Lambda_{\sigma^0}^{\text{DtN}}$. With noisy measurements, only a few, n singular values are above the noise level δ and we could choose the network $C((n-1)/2, n)$ with n boundary nodes. See [31, section 3.2.5] for more details.

5. Estimating the conductivity from the resistor network

Once we have determined the resistor network, the data fitting is done. Now we wish to estimate σ from the network. We do this by solving a nonlinear minimization problem introduced in section 5.1, using an iterative, Gauss–Newton method. We start the iteration with a good initial guess obtained from the network, as explained in section 5.3. The details of the iterative estimation of σ are given in section 5.4.

5.1. Outline of the method

To avoid confusion, let us denote here by σ^* the true and unknown conductivity function. We propose to estimate it by the minimizer of the objective function

$$\mathcal{O}(\sigma) = \frac{1}{2} \|\Gamma_n(\sigma) - \Gamma_n(\sigma^*)\|_2^2. \quad (20)$$

The minimization is done over the set \mathcal{S} of positive and bounded conductivities and Γ_n is the composition of two maps

$$\Gamma_n(\sigma) = \mathcal{Q}_n \circ \mathcal{F}_n(\sigma). \quad (21)$$

Here \mathcal{F}_n is the forward map $\mathcal{F}_n : \mathcal{S} \rightarrow \mathcal{D}_n$, which takes $\sigma \in \mathcal{S}$ and maps it to

$$\mathcal{F}_n(\sigma) = \mathcal{M}_n(\Lambda_\sigma^{\text{DtN}}) \in \mathcal{D}_n, \quad (22)$$

the predicted measurements belonging to the set \mathcal{D}_n of DtN maps of well-connected, circular networks (see theorem 1 and definition 3). The map \mathcal{Q}_n in (21) takes these measurements to a set $\mathcal{S}_n \subset \mathbb{R}^{n(n-1)/2}$ of parametrized conductivities. We define it using the resistor network (reduced model) as follows.

Definition 2 (Mapping \mathcal{Q}_n). *Let \mathbf{A} be a matrix belonging to the set \mathcal{D}_n . Find the critical circular resistor network $C(l, n)$ with resistors $R_{i,j}$, $\widehat{R}_{i,j+1/2}$ and DtN map \mathbf{A} . Here $l = (n-1)/2$ and n is odd. Similarly find the resistor network $C^0(l, n)$ with DtN map $\mathcal{M}_n(\Lambda_{\sigma^0}^{\text{DtN}})$ for the reference, uniform conductivity $\sigma^0 \equiv 1$. This gives resistors R_i^0 , \widehat{R}_i^0 that can be regarded as constants. The map $\mathcal{Q}_n : \mathcal{D}_n \rightarrow \mathcal{S}_n$ takes the data matrix \mathbf{A} to the parametrized conductivities*

$$\begin{aligned} \widehat{\sigma}_{i,j} &= \frac{R_i^0}{R_{i,j}} & i = 1, \dots, \lfloor l/2 \rfloor, & \quad j = 1, \dots, n, \\ \sigma_{i,j+1/2} &= \frac{\widehat{R}_i^0}{\widehat{R}_{i,j+1/2}} & i = 2, \dots, \lfloor l/2 \rfloor + 1, & \quad j = 1, \dots, n. \end{aligned} \quad (23)$$

We note that our inversion method is quite different from the typical output least squares formulation, which minimizes over σ the misfit between the measured data and the prediction of the forward map. Such a minimization is typically not well conditioned and it requires

careful regularization. Even then, convergence may be slow and the computational cost is high in comparison with that of our method. We illustrate this with numerical results in section 6.

The map \mathcal{Q}_n is used in the objective function (20) as a preconditioner of the forward map. This is the key point of our algorithm as we discuss next.

5.2. Preconditioning of the forward map using the adaptive grid $\mathcal{G}^0(l, n)$

Definition 2 of the map $\mathcal{Q}_n(\sigma)$ involves the ratio of two kinds of resistors: (1) the resistors R_{ij} and $\hat{R}_{i,j+1/2}$ in the network $C(l, n)$ for σ and (2) the resistors R_i^0 and \hat{R}_i^0 in the network $C^0(l, n)$ for the reference conductivity $\sigma^0 = 1$, given by (18) in terms of the primary and dual radii in the adaptive grid $\mathcal{G}^0(l, n)$. As explained in section 3.2.3 (see equations (11), (12)), R_{ij} and $\hat{R}_{i,j+1/2}$ can be interpreted as averages of σ on cells of an appropriate discretization grid. The key point in definition 1 is that $\mathcal{G}^0(l, n)$ is such a grid.

Now, imagine that we took the approximate averages of σ returned by \mathcal{Q}_n and interpolated them on the grid $\mathcal{G}^0(l, n)$, with some interpolation operator $\mathcal{P} : \mathcal{S}_n \rightarrow \mathcal{S}$. We would get that for smooth enough conductivities

$$\mathcal{P} \circ \mathcal{Q}_n(\mathcal{M}_n(\Lambda_\sigma^{\text{DtN}})) \approx \sigma, \quad (24)$$

and therefore that $\mathcal{P} \circ \mathcal{Q}_n$ would be an approximate inverse of the forward map

$$\mathcal{F}_n(\sigma) = \mathcal{M}_n(\Lambda_\sigma^{\text{DtN}}).$$

Put otherwise, $\mathcal{P} \circ \Gamma_n$ would be close to an identity for such σ and the minimization of (20) would become trivial, because of the preconditioning role played by \mathcal{Q}_n .

We illustrate all these points with numerical simulations in the following section. But before that, let us discuss some theoretical results.

5.2.1. Necessary condition for convergence. To prove convergence of our method, we would need to show that it is both necessary and sufficient that the inversion be done on the reference grid $\mathcal{G}^0(l, n)$. Here we give the necessary condition. Sufficiency remains a conjecture at this point but it was established in [10] for a closely related problem in layered media, where we have different (spectral) measurements of the DtN map.

Consider a compact set \mathcal{S} of sufficiently smooth conductivity functions and let $\sigma^0 \in \mathcal{S}$. Consider also an arbitrary tensor product grid $\mathcal{G}(l, n)$ and define $\epsilon_l > 0$ as the smallest real number so that

$$\begin{aligned} \max_{\sigma \in \mathcal{S}} \max_{1 \leq j \leq n} h_\theta \left| \int_{r_{i+1}}^1 dr \left(r \int_{(j-1/2)h_\theta}^{(j+1/2)h_\theta} d\theta \sigma(r, \theta) \right)^{-1} - \sum_{p=1}^i R_{p,j} \right| &\leq \epsilon_l, \quad i = 1, \dots, \lceil l/2 \rceil \\ \max_{\sigma \in \mathcal{S}} \max_{1 \leq j \leq n} \left| \frac{1}{h_\theta} \int_{\hat{r}_i}^1 dr \int_{jh_\theta}^{(j+1)h_\theta} d\theta \frac{\sigma(r, \theta)}{r} - \sum_{p=2}^i \frac{h_\theta}{\hat{R}_{i,j+1/2}} \right| &\leq \epsilon_l, \quad i = 2, \dots, \lfloor l/2 \rfloor + 1. \end{aligned}$$

Here ϵ_l is necessarily bounded, because $\sigma(r, \theta)$ is bounded and strictly positive. The resistors are defined for each $\sigma \in \mathcal{S}$, by solving problem 1 with data $\mathcal{M}_n(\Lambda_\sigma^{\text{DtN}})$.

Now, suppose that there exist tensor product grids that are nearly optimal for all $\sigma \in \mathcal{S}$, in the asymptotic limit $l \rightarrow \infty$. The following proposition shows that they are necessarily close to the optimal grid for the reference conductivity σ^0 .

Proposition 1. *If there exist grids $\mathcal{G}(l, n)$ so that $\epsilon_l \rightarrow 0$ as $l \rightarrow \infty$, then they must be asymptotically close to the optimal grid $\mathcal{G}^0(l, n)$.*

Proof. The proof is trivial. Since $\sigma^0 \in \mathcal{S}$ and $\sigma^0 = 1$, we obtain

$$\begin{aligned} \max_{\sigma \in \mathcal{S}} \max_{1 \leq j \leq n} h_\theta \left| \int_{r_{i+1}}^1 dr \left(r \int_{(j-1/2)h_\theta}^{(j+1/2)h_\theta} d\theta \sigma(r, \theta) \right)^{-1} - \sum_{p=1}^i R_{p,j} \right| \\ \geq \max_{1 \leq j \leq n} h_\theta \left| \int_{r_{i+1}}^1 dr \left(r \int_{(j-1/2)h_\theta}^{(j+1/2)h_\theta} d\theta \sigma^0(r, \theta) \right)^{-1} - \sum_{p=1}^i R_{p,j}^0 \right| = |\ln r_{i+1} - \ln r_{i+1}^0|. \end{aligned}$$

Similarly,

$$\max_{\sigma \in \mathcal{S}} \max_{1 \leq j \leq n} \left| \frac{1}{h_\theta} \int_{\hat{r}_i}^1 dr \int_{jh_\theta}^{(j+1)h_\theta} d\theta \frac{\sigma(r, \theta)}{r} - \sum_{p=2}^i \frac{h_\theta}{\hat{R}_{i,j+1/2}} \right| \geq |\ln \hat{r}_i - \ln \hat{r}_i^0|.$$

Now by assumption

$$\begin{aligned} |\ln r_{i+1} - \ln r_{i+1}^0| &\leq \epsilon_l, & i = 1, \dots, \lfloor l/2 \rfloor \\ |\ln \hat{r}_i - \ln \hat{r}_i^0| &\leq \epsilon_l, & i = 2, \dots, \lfloor l/2 \rfloor + 1 \end{aligned}$$

and $\epsilon_l \rightarrow 0$ as $l \rightarrow \infty$. Thus grids $\mathcal{G}(l, n)$ must be asymptotically close to $\mathcal{G}^0(l, n)$. \square

5.3. Using the grid $\mathcal{G}^0(l, n)$ to obtain the initial guess for the Gauss–Newton iteration

We begin the iteration for minimizing the objective function (20) with the initial guess $\sigma_0(\mathbf{x})$ given by the linear interpolation of the discrete parameters returned by $\mathcal{Q}_n(\mathcal{M}_n(\Lambda_{\sigma^*}^{\text{DtN}}))$. Here $\mathcal{M}_n(\Lambda_{\sigma^*}^{\text{DtN}})$ is our data, corresponding to the true and unknown conductivity σ^* . The interpolation is done on the homogeneous grid $\mathcal{G}^0(l, n)$, as follows: we interpret $\hat{\sigma}_{i,j}$ and $\sigma_{i,j+1/2}$ as point values at (\hat{r}_i^0, jh_θ) and $(r_i^0, (j+1/2)h_\theta)$ respectively and then, we interpolate linearly using a Delaunay triangulation. Outside the convex hull of the evaluation points, we extrapolate linearly to get values over the whole Ω .

Note that once we have the resistors, it is trivial to compute the initial guess. But how close is it to the linear interpolation of the averages of the true conductivity σ^* on the grid $\mathcal{G}^0(l, n)$? If these two are close, then the grid $\mathcal{G}^0(l, n)$ is close to optimal, for the unknown σ^* . We demonstrate this in the following sections with numerical experiments.

5.3.1. Numerical results. We compute the initial guess from synthetic data sets for the conductivities shown in figure 5 and defined in appendix B.1. Then, we compare the result with the linear interpolation of the averages of σ^* on $\mathcal{G}^0(l, n)$,

$$\begin{aligned} \hat{\sigma}_{i,j}^* &= \frac{\ln(r_i^0/r_{i+1}^0)}{h_\theta} \left(\int_{r_{i+1}^0}^{r_i^0} dt \left(t \int_{(j-1/2)h_\theta}^{(j+1/2)h_\theta} \sigma^*(t, \theta) d\theta \right)^{-1} \right)^{-1}, \\ \sigma_{i,j+1/2}^* &= \frac{h_\theta}{\ln(\hat{r}_{i-1}^0/\hat{r}_i^0)} \left(\int_{jh_\theta}^{(j+1)h_\theta} d\theta \left(\int_{\hat{r}_{i-1}^0}^{\hat{r}_i^0} \frac{dt \sigma^*(t, \theta)}{t} \right)^{-1} \right)^{-1}. \end{aligned} \quad (25)$$

The comparison is done in figures 6 and 7 for noiseless measurements and on two grids: $\mathcal{G}^0(7, 15)$ and $\mathcal{G}^0(5, 11)$. The results for noisy measurements are in figures 8 and 9. We superpose the grid \mathcal{G}^0 on the plots and use the following convention: the primary grid is in solid lines and the dual grid is in dotted lines.

The data is obtained as follows: we discretize equation (1) with finite volumes, on a grid with 100×100 dual cells of uniform size and with constant conductivity over dual cells. This gives us approximate pointwise values of the kernel of the DtN map, at 100 equally spaced

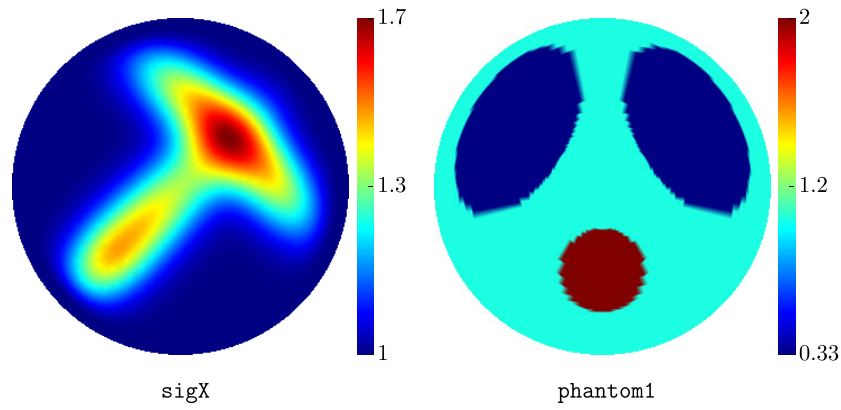


Figure 5. Conductivities used in the numerics. See appendix B.1 for definition.

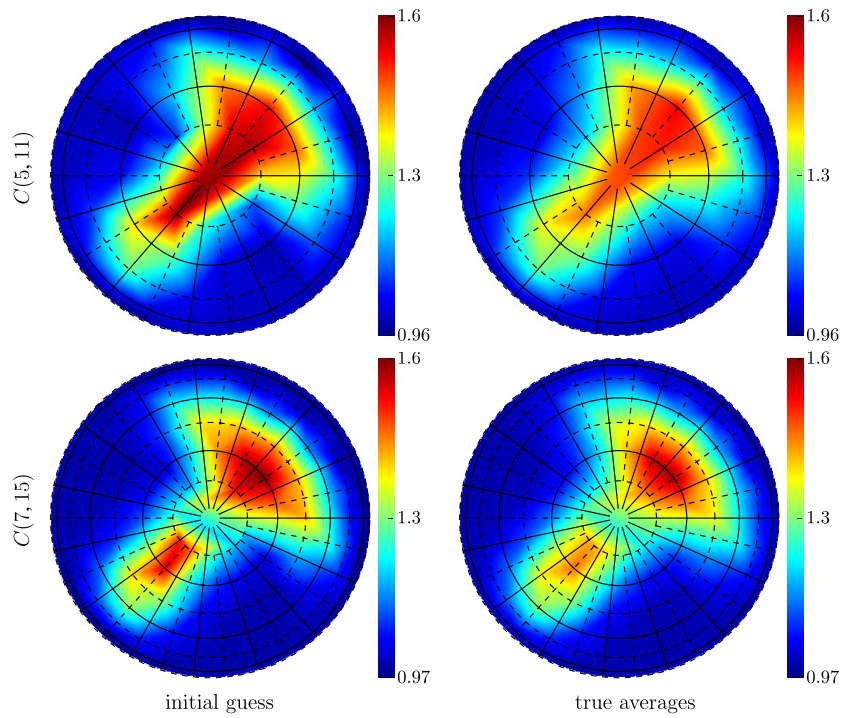


Figure 6. Left: initial guess for smooth conductivity sigX and noiseless data. Right: interpolation of the averages of sigX on \mathcal{G}^0 .

points of $\partial\Omega$. Then, we use these values in (7) to get the ‘measurements’ $\mathcal{M}_n(\Lambda_\sigma^{\text{DtN}})$ by lumping.

We simulate noise in the measurements by adding a multiplicative, mean zero Gaussian noise to the approximation of the kernel of the DtN map. We give in table 1 the size of the networks predicted by the SVD analysis of section 4.3, for different noise levels (see method 2 in section 4.3). This heuristic gives only approximate network sizes that do not always give positive resistors with the layer peeling algorithm that we used (see section 4.2).

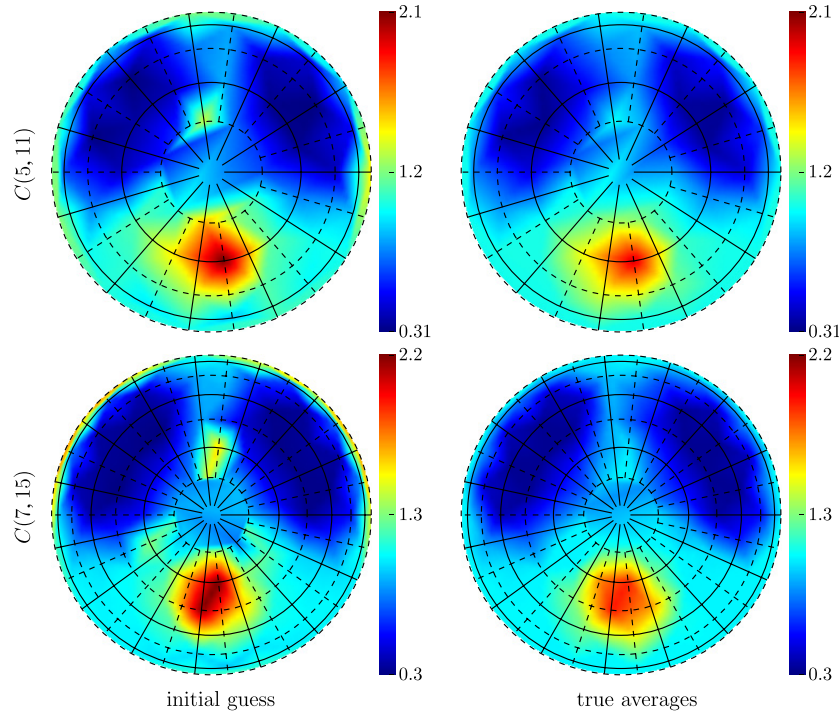


Figure 7. Left: initial guess for the piecewise constant conductivity `phantom1` and noiseless data. Right: interpolation of the averages of `phantom1` on \mathcal{G}^0 .

Table 1. Network sizes predicted by the SVD analysis of the NtD map.

	0.1%	0.5%	1%	5%
sigX	$C(7, 15)$	$C(4, 9)$	$C(3, 7)$	$C(1, 3)$
phantom1	$C(12, 25)$	$C(8, 17)$	$C(7, 15)$	$C(3, 7)$

This is why we preferred to find empirically the largest network that gives positive resistors for several realizations of the noise (see method 1 in section 4.3).

5.3.2. Other studies of the interpolation property of the grid $\mathcal{G}^0(l, n)$. The results in figures 6–9 show that $\mathcal{G}^0(l, n)$ is close to optimal for our test conductivities. Further evidence of this fact can be obtained from the sensitivity analysis of the map Γ_n .

Let $\delta\sigma$ be a perturbation of $\sigma^0 = 1$. The induced perturbation of Γ_n is

$$\Gamma_n(\sigma^0 + \delta\sigma) = \Gamma_n(\sigma^0) + D\Gamma_n[\sigma^0]\delta\sigma + \dots, \quad (26)$$

where $D\Gamma_n[\sigma^0]$ is the formal Jacobian of Γ_n at σ^0 . If it is true that we can make the approximations

$$\begin{aligned} \hat{\sigma}_{i,j} &= \frac{R_i^0}{R_{i,j}} \approx \frac{\ln(r_i^0/r_{i+1}^0)}{h_\theta} \left(\int_{r_{i+1}^0}^{r_i^0} dt \left(t \int_{(j-1/2)h_\theta}^{(j+1/2)h_\theta} \sigma(t, \theta) d\theta \right)^{-1} \right)^{-1}, \\ \sigma_{i,j+1/2} &= \frac{\hat{R}_i^0}{\hat{R}_{i,j+1/2}} \approx \frac{h_\theta}{\ln(\hat{r}_{i-1}^0/\hat{r}_i^0)} \left(\int_{jh_\theta}^{(j+1)h_\theta} d\theta \left(\int_{\hat{r}_i^0}^{\hat{r}_{i-1}^0} dt \frac{\sigma(t, \theta)}{t} \right)^{-1} \right)^{-1}, \end{aligned} \quad (27)$$

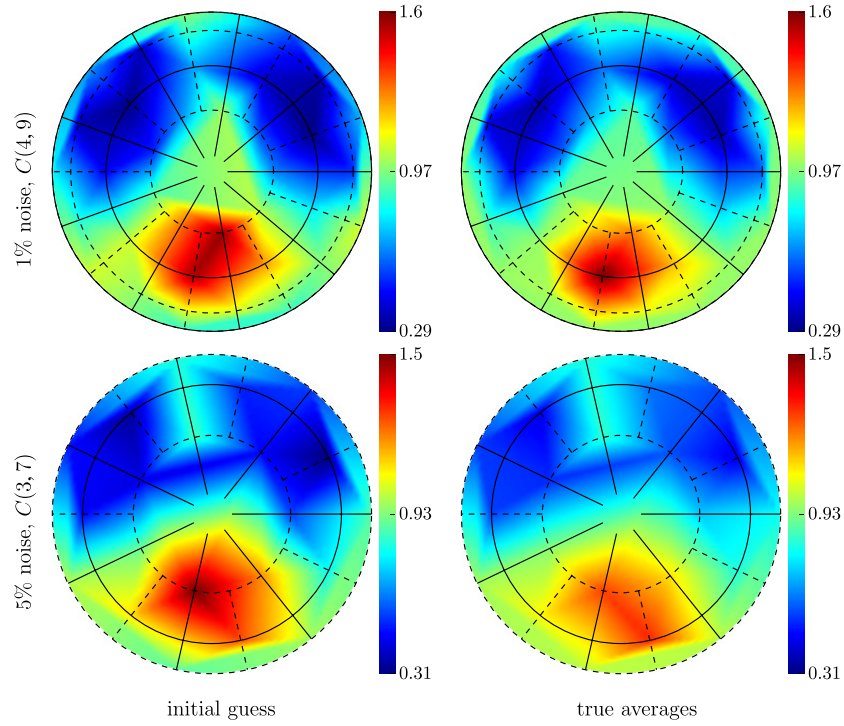


Figure 8. Left: initial guess for the piecewise constant conductivity phantom1 and noisy data. Right: interpolation of the averages of phantom1 on \mathcal{G}^0 .

for $\sigma = \sigma^0 + \delta\sigma$, then the sensitivity functions of $\Gamma_n(\sigma)$ would be close to the indicator functions of the cells in \mathcal{G}^0 . We plot a few sensitivity functions in figure 10 and observe that this is indeed the case, as they are all nicely localized around the grid cells.

5.4. The Gauss–Newton iteration

Given measurements $\mathcal{M}_n(\Lambda_{\sigma^*}^{\text{DtN}})$, we use the Gauss–Newton method to find σ that minimizes (20). Convergence of Gauss–Newton for EIT is considered in [26]. The analysis for our method is similar, since \mathcal{Q}_n is an invertible mapping, and so is its differential [19]. From results such as [23, section 4.4], we expect local convergence of the method to σ that fits the measurements (assuming that $D\Gamma_n[\sigma]$ has full row rank).

Now the conductivity must remain positive and we enforce this constraint by changing variables $\kappa = \ln(\sigma)$. Because we wish to compare quantities that are as similar as possible to our new variable κ , we modify slightly the objective function, by taking the logarithm of Γ_n . This takes us to the unconstrained minimization,

$$\min_{\kappa} \frac{1}{2} \|\tilde{\Gamma}_n(\kappa) - \tilde{\Gamma}_n(\kappa^*)\|_2^2, \quad (28)$$

where $\tilde{\Gamma}_n \equiv \ln \circ \Gamma_n \circ \exp$ and $\kappa^* = \ln(\sigma^*)$. We compute sensitivity functions for the mapping $\tilde{\Gamma}_n$, with respect to perturbations of the log-conductivity κ , and obtain the formal expansion,

$$\tilde{\Gamma}_n(\kappa + \delta\kappa) = \tilde{\Gamma}_n(\kappa) + D\tilde{\Gamma}_n[\kappa]\delta\kappa + \cdots. \quad (29)$$

Here $D\tilde{\Gamma}_n[\kappa]$ is the Jacobian of $\tilde{\Gamma}_n$ evaluated at κ .

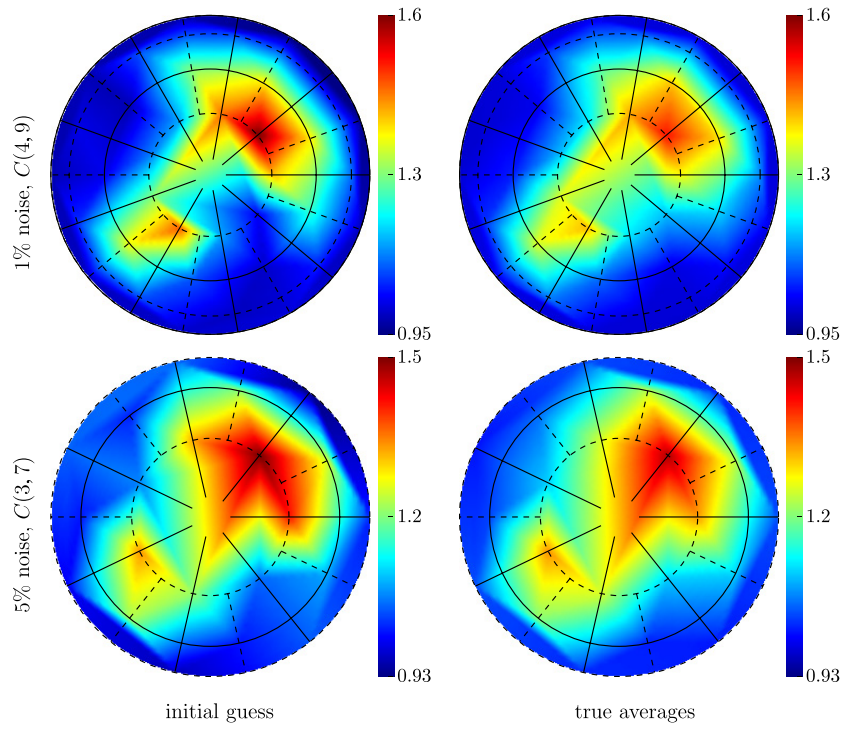


Figure 9. Left: initial guess for the smooth conductivity sigX and noisy data. Right: interpolation of averages of sigX on \mathcal{G}^0 .

The Gauss–Newton method consists of finding the new iterate κ_{j+1} , from the previous iterate κ_j , by

$$\kappa_{j+1} = \kappa_j + (D\tilde{\Gamma}_n[\kappa_j])^\dagger (\tilde{\Gamma}_n(\kappa^*) - \tilde{\Gamma}_n(\kappa_j)), \quad (30)$$

where $(D\tilde{\Gamma}_n[\kappa_j])^\dagger$ is the pseudo-inverse⁶ of $D\tilde{\Gamma}_n[\kappa_j]$. This iteration amounts to finding the update $\delta\kappa = \kappa_{j+1} - \kappa_j$ as the minimal L^2 norm solution of the normal equations,

$$D\tilde{\Gamma}_n^*[\kappa_j] D\tilde{\Gamma}_n[\kappa_j] \delta\kappa = D\tilde{\Gamma}_n^*[\kappa_j] (\tilde{\Gamma}_n(\kappa^*) - \tilde{\Gamma}_n(\kappa_j)),$$

where $D\tilde{\Gamma}_n^*[\kappa_j]$ is the adjoint of $D\tilde{\Gamma}_n[\kappa_j]$. In other words, we find the *orthogonal projection* of the update $\delta\kappa = \kappa_{j+1} - \kappa_j$ onto the span of the sensitivity functions. Implicitly this is a form of regularization.

We start the iterations with the initial guess obtained as in section 5.3. That this initial guess is close to σ^* is helpful in the convergence, as expected. The algorithm is summarized below and numerical experiments are shown in section 6.

Algorithm 1. *Inputs:* Measurements $\mathcal{M}_n(\Lambda_{\sigma^*}^{DtN})$ (definition 1) for n odd and some tolerance ϵ for stopping the iteration. *Outputs:* An estimate of the conductivity.

- (1) Compute $\kappa_0 = \ln(\sigma_0)$, where σ_0 is obtained as in section 5.3 by interpolating the output of \mathcal{Q}_n applied to $\mathcal{M}_n(\Lambda_{\sigma^*}^{DtN})$, on the homogeneous conductivity grid.
- (2) For $j = 0, 1, \dots$ do,

⁶ The pseudo-inverse or Moore–Penrose generalized inverse can be defined in the context of the Hilbert spaces, see e.g. [29, section 2].

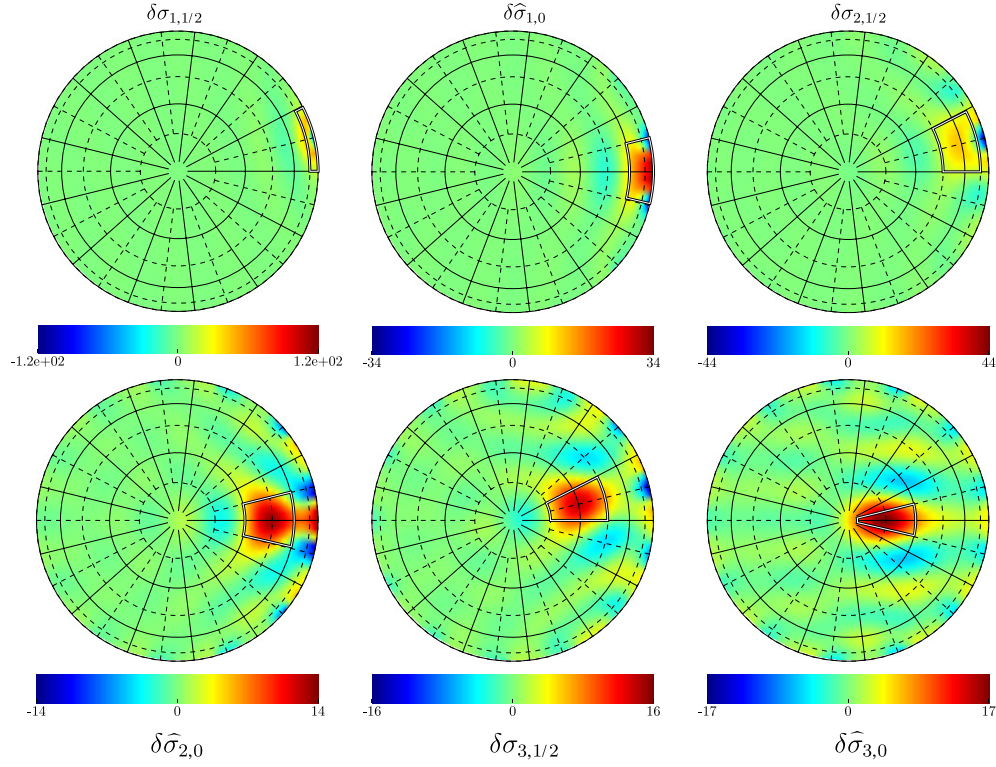


Figure 10. Sensitivity of $\Gamma_n(\sigma)$ to perturbations of σ . The resistor network is $C(6, 13)$ and the reference conductivity is $\sigma^0 \equiv 1$. Since there is a $2\pi/13$ rotational symmetry, we plot only sensitivities for $\sigma_{i,1/2}$ and $\hat{\sigma}_{i,0}$. All the sensitivity functions integrate to one. We highlight the cells where we average.

- (a) $\kappa_{j+1} \leftarrow \kappa_j + (D\tilde{\Gamma}_n[\kappa_j])^\dagger (\tilde{\Gamma}_n(\kappa^*) - \tilde{\Gamma}_n(\kappa_j))$
 (b) If $\|\tilde{\Gamma}_n(\kappa_{j+1}) - \tilde{\Gamma}_n(\kappa^*)\|_2 < \epsilon$, stop.
 (3) Estimate σ^* by $\exp(\kappa_{j+1})$.

6. Numerical results

6.1. Implementation of the Gauss–Newton algorithm

In our numerical experiments, n is much smaller than the number of parameters used for discretizing κ . Thus, the pseudo-inverse in the Gauss–Newton iteration (30) can be computed efficiently, with the identity

$$(D\tilde{\Gamma}_n[\kappa_j])^\dagger = D\tilde{\Gamma}_n^*[\kappa_j](D\tilde{\Gamma}_n[\kappa_j]D\tilde{\Gamma}_n^*[\kappa_j])^\dagger. \quad (31)$$

The Jacobian $D\tilde{\Gamma}_n[\kappa_j]$ was full-rank to working precision and well conditioned, for all the σ^* that we tried. This made the small matrix $D\tilde{\Gamma}_n[\kappa_j]D\tilde{\Gamma}_n^*[\kappa_j]$ invertible and, therefore, the pseudo-inverse in (31) could be replaced by solving a small linear system.

In general, one uses globalization strategies, such as line search or trust region, to guarantee progress at each iteration of algorithm 1, by essentially limiting the size of the update of κ (see

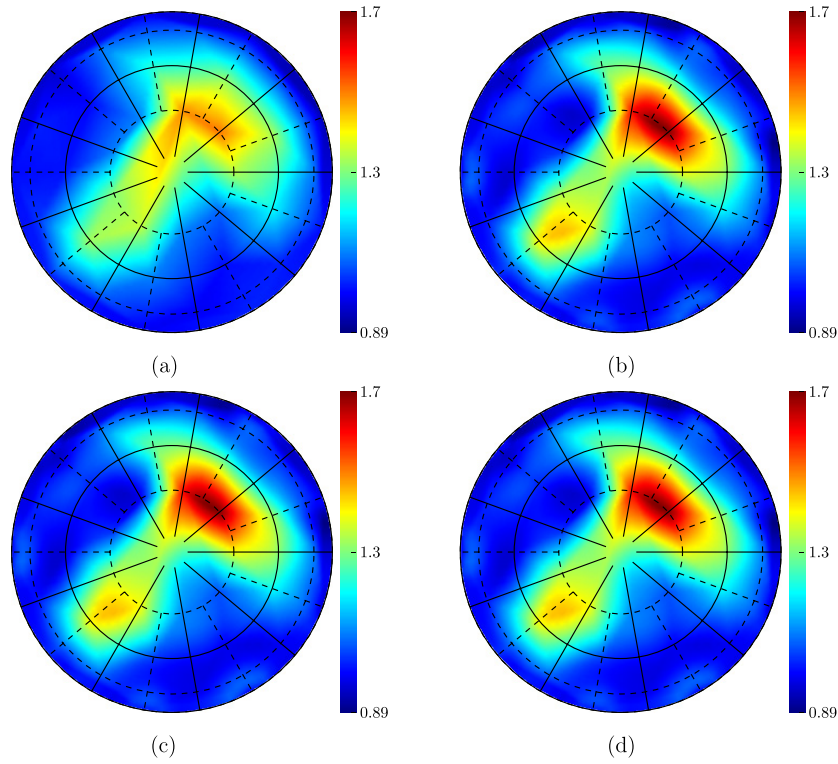


Figure 11. Convergence history for algorithm 1 on the conductivity sigX , with 1% noise. The reported residual is the misfit $\|\tilde{\Gamma}_n(\ln(\sigma)) - \tilde{\Gamma}_n(\ln(\sigma^*))\|_2^2$. (a) Initial guess σ_0 , residual = 1.03×10^{-1} ; (b) iterate σ_1 , residual = 1.00×10^{-4} ; (c) iterate σ_2 , residual = 6.62×10^{-11} ; (d) iterate σ_3 , residual = 1.70×10^{-23} .

e.g. [41, chapters 3, 4]). We did not need such strategies, probably because the initial iterate (see section 5.3) was always close enough to σ^* .

6.2. The results

We give in figures 11 and 12 two typical images obtained with algorithm 1, on data collected with 100 ‘electrodes’ tainted with 1% multiplicative, mean zero, Gaussian noise. As we can see from the results, numerical convergence occurs in only a few iterations, with the largest update done in the first iteration. For all practical purposes, this first iterate is already a good image. Note that the conductivity values are better resolved after the iteration than in the initial guess σ_0 .

6.3. A nonlinear preconditioning of the problem?

If we follow the traditional approach of minimizing directly the misfit in the measurements with the Gauss–Newton method, we obtain an iteration with the Jacobian $D\mathcal{F}_n[\sigma]$ of the forward map $\mathcal{F}_n(\sigma) = \mathcal{M}_n(\Lambda_\sigma^{\text{DIN}})$, instead of $D\Gamma_n(\sigma) = D\mathcal{Q}_n[\mathcal{F}_n(\sigma)]D\mathcal{F}_n[\sigma]$. We compare the condition numbers (ratio of largest to smallest singular value) of these two Jacobians in table 2. Note that in all the cases we considered, the matrices approximating these quantities were full-rank, so that when using identity (31), the condition number of the systems we

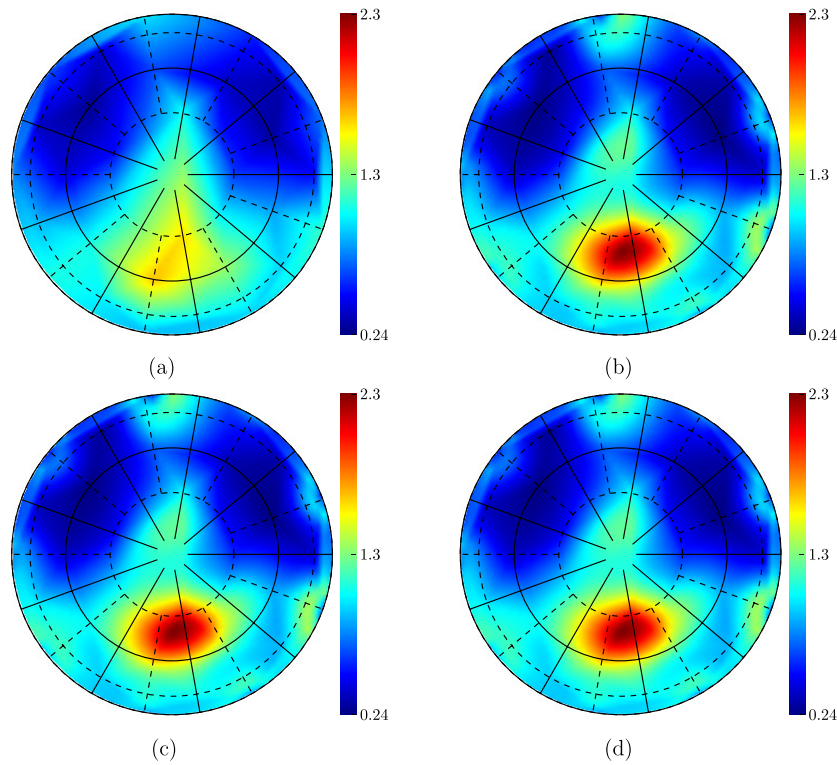


Figure 12. Convergence history for algorithm 1 on the conductivity phantom1, with 1% noise. The reported residual is the misfit $\|\tilde{\Gamma}_n(\ln(\sigma)) - \tilde{\Gamma}_n(\ln(\sigma^*))\|_2^2$. (a) Initial guess σ_0 , residual = 7.61×10^{-1} ; (b) iterate σ_1 , residual = 3.10×10^{-3} ; (c) iterate σ_2 , residual = 2.29×10^{-8} ; (d) iterate σ_3 , residual = 7.73×10^{-18} .

Table 2. Condition numbers of $D\Gamma_n[\sigma]$ and $D\mathcal{F}_n[\sigma]$, for different conductivities.

n	$\sigma \equiv 1$		$\sigma \equiv \text{sigX}$		$\sigma \equiv \text{phantom1}$	
	$D\mathcal{F}_n[\sigma]$	$D\Gamma_n[\sigma]$	$D\mathcal{F}_n[\sigma]$	$D\Gamma_n[\sigma]$	$D\mathcal{F}_n[\sigma]$	$D\Gamma_n[\sigma]$
9	5.55×10^2	4.81×10^0	5.72×10^2	4.80×10^0	1.24×10^3	4.48×10^0
11	5.14×10^3	6.01×10^0	5.27×10^3	5.92×10^0	1.13×10^4	5.67×10^0
13	4.88×10^4	7.89×10^0	4.95×10^4	7.78×10^0	9.19×10^4	7.56×10^0

need to solve to compute the Gauss–Newton update, is actually the square of what appears in table 2.

We observe that the condition numbers of $D\Gamma_n[\sigma]$ are orders of magnitude smaller than those of $D\mathcal{F}_n[\sigma]$, and that they do not change considerably with n or the conductivity. This is numerical evidence that the mapping \mathcal{Q}_n (see definition 2) preconditions the problem.

7. Using *a priori* information about the conductivity

If *a priori* information about σ^* is available, it should be taken into account in the imaging process. Here we show how to incorporate a certain type of prior information, which says that

σ^* is ‘blocky’, or piecewise constant. We do this using a penalty function $J(\kappa) = \text{TV}(\kappa)$ on the total variation semi-norm of the log-conductivity.

The Gauss–Newton iteration of section 6 uses no prior information and it converges very fast. In fact, we saw that after the first iteration, the corrections were negligible and the image remained virtually unchanged. Therefore, for all practical purposes it is enough to keep the first Gauss–Newton iterate. This is the same as finding the minimal $L^2(\Omega)$ norm solution $\tilde{\kappa}$ of the linearized problem

$$D\tilde{\Gamma}_n[\kappa_0](\tilde{\kappa} - \kappa_0) = \tilde{\Gamma}_n(\kappa^*) - \tilde{\Gamma}_n(\kappa_0), \quad (32)$$

with respect to the initial guess σ_0 defined in section 5.3. The solution $\tilde{\kappa}$ gives a perfect data fit, by design, to the linearized problem. Now, we wish to improve it, using the prior information.

Note that $\kappa = \tilde{\kappa} + \delta\kappa$ is also a solution of (32), provided that $\delta\kappa \in \text{null}(D\tilde{\Gamma}_n[\kappa_0])$. This means that we can add *a priori* information by simply looking for the correction $\delta\kappa$ in the orthogonal complement of the sensitivity functions (i.e. $\text{null}(D\tilde{\Gamma}_n[\kappa_0])$) that minimizes the penalty functional $J(\kappa)$. This gives the constrained optimization problem,

$$\begin{aligned} \min_{\kappa} \quad & J(\kappa) \\ \text{subject to} \quad & D\tilde{\Gamma}_n[\kappa_0](\kappa - \tilde{\kappa}) = 0. \end{aligned} \quad (33)$$

The procedure is summarized as follows.

Algorithm 2. *Inputs:* measurements $\mathcal{M}_n(\Lambda_{\sigma^*}^{\text{DtN}})$ for n odd and the penalty functional $J(\kappa)$ encoding the *a priori* information. *Outputs:* an estimate of the conductivity.

- (1) Compute $\kappa_0 = \ln(\sigma_0)$, where σ_0 is obtained as in section 5.3 by interpolating the output of \mathcal{Q}_n applied to $\mathcal{M}_n(\Lambda_{\sigma^*}^{\text{DtN}})$, on the homogeneous conductivity grid.
- (2) Carry out the first iteration of algorithm 1,

$$\tilde{\kappa} \leftarrow \kappa_0 + (D\tilde{\Gamma}_n[\kappa_0])^\dagger (\tilde{\Gamma}_n(\kappa^*) - \tilde{\Gamma}_n(\kappa_0)).$$

- (3) Estimate $\kappa^* = \ln(\sigma^*)$ by the minimizer of ((33))

Imaging with a total variation penalty was done before, for example by Dobson and Santosa [27]. However, this was coupled with traditional output least squares, where σ was sought directly as a minimizer of the data misfit. In such cases, the constraints are the sensitivities of the *data* to perturbations of σ . The sensitivity matrices are typically ill-conditioned, so an SVD truncation is required [27]. In our approach, the sensitivity matrix $D\tilde{\Gamma}_n[\kappa_0]$ has a small condition number, as explained in section 5.4 and optimization (33) is easier to do. This is especially because we have small resistor networks and, therefore, few constraints.

7.1. Numerical experiments with *a priori* information

We implemented algorithm 1 with the total variation penalty function

$$J_{\text{TV}}(\kappa) = \text{TV}(\kappa), \quad \text{where} \quad \text{TV}(\kappa) = \int_{\Omega} \|\nabla \kappa(\mathbf{x})\|_2 \, d\mathbf{x}.$$

7.1.1. Implementation strategies. To solve problem (33) we resort to an SQP (sequential quadratic programming) method where the KKT (Karush–Kuhn–Tucker) systems are solved using the range space approach [41, chapter 18]. This method is well suited for our optimization problem, because we have only a few linear constraints, and the Hessian of the Lagrangian of (33) is readily available, positive definite and sparse. For the size of the problems we

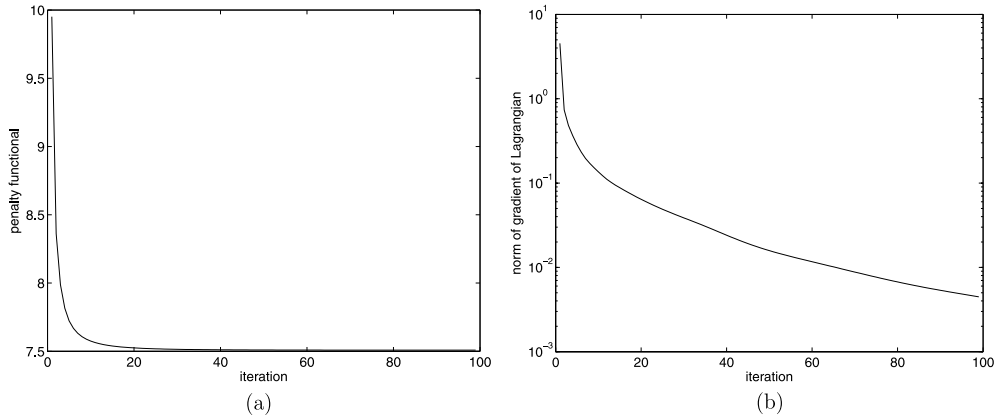


Figure 13. Typical convergence history of the SQP algorithm for minimizing (33) with a TV penalty functional. (a) Penalty functional; (b) norm of gradient of the Lagrangian.

considered (up to 10^4 variables for σ), sparse direct methods (such as UMFPACK in Matlab) are efficient in solving the systems involving the Hessian that need to be computed at each iteration of the optimization algorithm.

To make the convergence global, we control the size of the step with a line search strategy on an ℓ_1 -type merit function [41, p 544]. Moreover, to minimize the non-differentiable functional J_{TV} we use the standard trick of approximating the absolute value by a smooth functional,

$$TV(\kappa) \approx \int_{\Omega} \sqrt{\|\nabla \kappa(\mathbf{x})\|_2^2 + \beta^2} d\mathbf{x},$$

with $\beta = 0.1$. We also use the quasi-Newton approximation of the Hessian of the TV functional (i.e. neglecting the part of the Hessian containing second derivatives), that is further regularized by adding 10^{-2} to the diagonal entries. This additional regularization also controls the step length.

The resulting numerical method for minimizing (33), with the J_{TV} penalty function, is very similar to the so-called lagged diffusivity method [47, p 136], modified to take into account the constraints.

7.1.2. Noiseless reconstructions. We stopped the iterations when the norm of the gradient of the Lagrangian was reduced by a factor of 5×10^{-2} , which in all our test cases occurred in no more than 15 SQP iterations. As seen in figure 13, a typical convergence justifies our stopping criterion: much of the progress in reducing the objective function is done at the beginning, so it is best to terminate the iterations early.

We present in figure 14 images of σ on a uniform grid with 50×50 cells. The noiseless data are computed numerically as explained in section 5.3.1.

7.2. Comparison of our method to output least squares

We compare our approach to traditional output least squares (LS) in figure 15. Both methods are given the same noisy data collected at 50 ‘electrodes’.

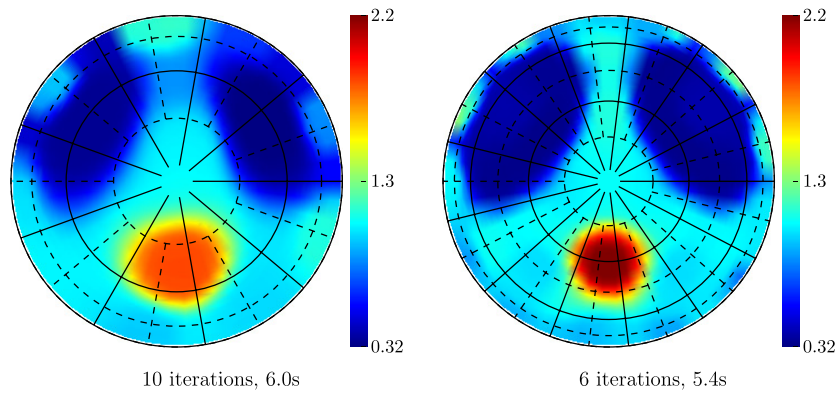


Figure 14. Images from noiseless data, using algorithm 2, with TV penalty functional and for conductivity `phantom1`. We show the results given by two resistor networks.

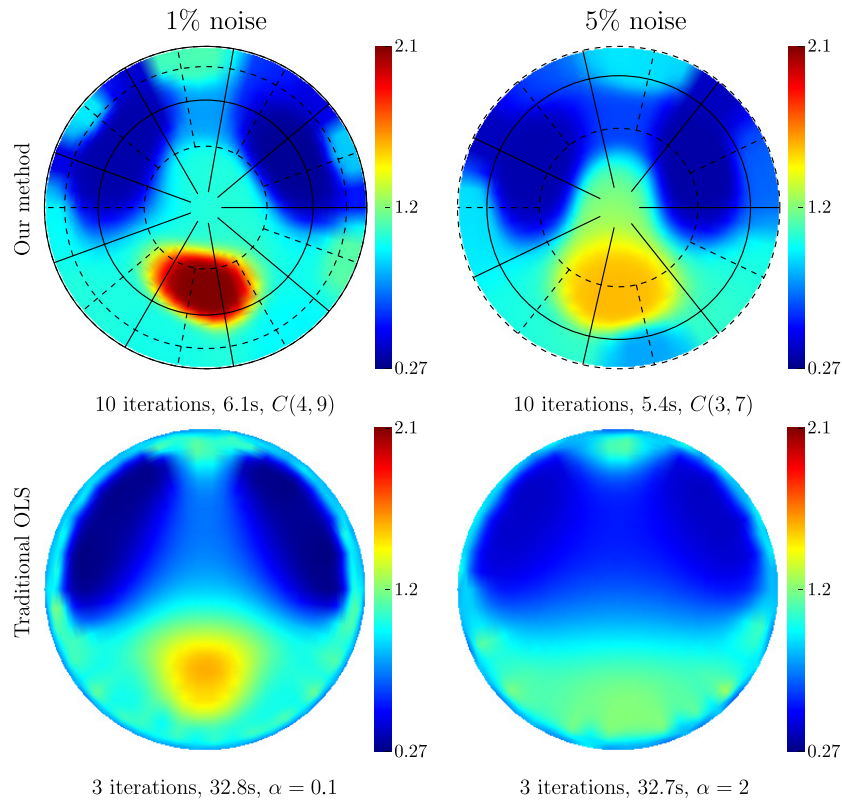


Figure 15. Comparison with traditional output least squares. The same color scale is used for all four reconstructions.

To be more specific, let N be the number of electrodes and $\mathcal{M}_N(\Lambda_\sigma^{\text{DtN}})$ the measured DtN map. In the LS method, we seek the log-conductivity κ^* minimizing,

$$\min_{\kappa} \frac{1}{2} \left\| \mathcal{M}_N(\Lambda_{\exp(\kappa)}^{\text{DtN}}) - \mathcal{M}_N(\Lambda_{\sigma^*}^{\text{DtN}}) \right\|_F^2 + \alpha \text{TV}(\kappa), \quad (34)$$

where $\|\cdot\|_F$ is the Frobenius norm for matrices. We determine empirically the regularization parameter α by minimizing (34) for different values of α .

We minimize (34) using the quasi-Newton approximation of the Hessian of the TV penalty and we regularize further the Hessian by adding 10^{-3} to the diagonal entries. We use an Armijo line search [41, chapter 3] as a globalization strategy of the iterations. The stopping criterion was to achieve a relative reduction of the norm of the gradient by at least 10^{-2} . The conductivity is discretized on the same 50×50 cells of uniform size. This makes the Hessian of the objective function in (34) a 2501×2501 dense matrix that is formed explicitly in our code.

The times included in figures 14 and 15 correspond to wall-clock times for obtaining reconstructions in Matlab r2006a on a Pentium 4 Linux PC with 2 GB of RAM. We remark that algorithm 1 is roughly five times faster than the traditional LS approach. In our LS implementation, close to 50% of the time is spent forming the Hessian and solving for the Newton updates, while the other 50% corresponds to solving the forward problem and computing derivatives. Thus, LS would be more expensive than our approach even if we could find a more efficient way of computing the updates (e.g. with a Krylov-based iterative solver). The computational advantage of our approach is that we do not need to solve *at each iteration* the forward problem and compute derivatives.

Remark 3. We show in figure 15 the LS images on the *same color scale* as that for our method, for noise levels 1% and 5%. These reconstructions would be comparable to those in e.g. [12, 13, 15, 27, 37] if each image had its own color scale ranging from its minimum to maximum values. However since we are using here a color scale that is close to the range of the true σ^* , the LS reconstructions appear worse than those in [12, 13, 15, 27, 37].

8. Summary

We introduced a novel inversion approach for electrical impedance tomography in two dimensions. It consists of two key steps: in the first step, we look for a reduced model which fits the boundary measurements. This is a well-connected, critical resistor network that we prove is uniquely recoverable from the data. In the second step, we seek the conductivity from the reduced model, with a Newton-type iteration.

We use the resistor network to define a nonlinear mapping \mathcal{Q}_n of the data to the space of conductivities. This is an approximate inverse of the forward map \mathcal{F}_n , for a large class of conductivities. The Newton-type iteration is defined for the composition $\mathcal{Q}_n \circ \mathcal{F}_n$ of the two maps, which are approximate inverses of each other. This makes the problem well conditioned. We also use the map \mathcal{Q}_n to get a very good initial guess of the conductivity by interpolating on a grid that is adapted to the measurements for a reference conductivity. This leads to fast convergence of the Newton-type iteration.

The inversion method does not require *a priori* information of the conductivity. However, we show how to incorporate such information in the imaging process. We present numerical results and a comparison with the traditional output least squares approach.

Acknowledgments

The work of L Borcea was partially supported by the National Science Foundation, grants DMS-0305056, DMS-0354658 and DMS-0604008. F Guevara Vasquez was supported in part by the National Science Foundation grant DMS-0305056. He wishes to thank the Schlumberger-Doll Research Math and Modeling group for a research internship in the

Summer 2005. The authors thank Tarek Habashy, Aria Abubakar and Michael Zaslavsky for useful conversations.

Appendix A. Converting NtD map measurements to DtN map measurements using convex duality

We derive the simple relation (A.5) to get the measured DtN map for $1/\sigma$ from measurements of the NtD map for σ . If we are given NtD map measurements for σ , the idea is to use (A.5) to generate data for our inversion method. We would then get an image of $1/\sigma$ (and therefore its reciprocal, for σ) from such artificial data.

In two dimensions, the electric current density \mathbf{j} is divergence free, so there is a scalar field h such that $\mathbf{j} = -\nabla^\perp h$, where $\nabla^\perp \equiv (\partial/\partial y, -\partial/\partial x)^T$. The current density is related to the electric potential u through Ohm's law (see e.g. [6, section 2.1])

$$\sigma \nabla u = -\mathbf{j} = \nabla^\perp h. \quad (\text{A.1})$$

Now recall that the DtN map is defined as $\Lambda_\sigma^{\text{DtN}} f = \mathbf{n} \cdot (\sigma \nabla u)$ where u solves the differential equation with Dirichlet boundary conditions,

$$\nabla \cdot [\sigma \nabla u] = 0 \text{ in } \Omega \quad \text{and} \quad u|_{\partial\Omega} = f.$$

By the duality relation (A.1) we have that h solves the differential equation with Neumann boundary conditions,

$$\nabla \cdot \left[\frac{1}{\sigma} \nabla h \right] = 0 \text{ in } \Omega \quad \text{and} \quad \mathbf{n} \cdot \left(\frac{1}{\sigma} \nabla h \right) = -\mathbf{n} \cdot \nabla^\perp u \text{ on } \partial\Omega.$$

By using the duality relation (A.1) again we get that $\Lambda_\sigma^{\text{DtN}} f = \mathbf{n} \cdot \nabla^\perp h$. Since Ω is the unit disc, the tangential derivative takes the form $\mathbf{n} \cdot \nabla^\perp \equiv \partial/\partial\theta$ where θ is the angle parametrizing the unit circle in the usual way. Therefore the NtD map of $1/\sigma$ and the DtN map of σ are related via the duality relation,

$$\Lambda_\sigma^{\text{DtN}} = -\frac{\partial}{\partial\theta} \Lambda_{1/\sigma}^{\text{NtD}} \frac{\partial}{\partial\theta}. \quad (\text{A.2})$$

Our inversion algorithms assume measurements (7) of the DtN map. We now show using the duality relation (A.2), that NtD measurements consistent with the 'shunt electrode model' [43], can be transformed into DtN map measurements.

Let ψ_1, \dots, ψ_{2n} be $2n$ nonnegative functions in $H^{-1/2}(\partial\Omega)$ with disjoint supports, numbered in circular order around the boundary, and such that $\int_{\partial\Omega} \psi_i \, \mathrm{d}\mathbf{x} = 1$. Assume NtD map measurements in the form $\mathcal{M}_{2n}(\Lambda_\sigma^{\text{NtD}}) \in \mathbb{R}^{2n \times 2n}$, defined componentwise by

$$(\mathcal{M}_{2n}(\Lambda_\sigma^{\text{NtD}}))_{i,j} = \begin{cases} \langle \psi_i, \Lambda_\sigma^{\text{NtD}} \psi_j \rangle & \text{if } i \neq j, \\ -\sum_{p=1, p \neq i}^{2n} \langle \psi_i, \Lambda_\sigma^{\text{NtD}} \psi_p \rangle & \text{otherwise,} \end{cases} \quad (\text{A.3})$$

where $\langle \cdot, \cdot \rangle$ is the $H^{-1/2}(\partial\Omega), H^{1/2}(\partial\Omega)$ duality pairing. Let I_i be the smallest connected component of $\partial\Omega$ containing both $\text{supp } \psi_{2i}$ and $\text{supp } \psi_{2i-1}$, and the functions ζ_i be defined for $i = 1, \dots, n$ by

$$\zeta_i(\theta) = \int_{\alpha_i}^{\theta} [\psi_{2i-1}(s) - \psi_{2i}(s)] \, \mathrm{d}s.$$

Here α_i is the angle of some point in the complement of I_i in $\partial\Omega$. Thus since the functions ψ_k integrate to one, we have $\text{supp } \zeta_i = I_i$. Furthermore, the functions ζ_i are nonnegative because the ψ_k are numbered by increasing θ .

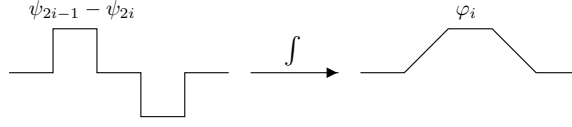


Figure A1. How n measurement functions φ_i for the DtN map could be obtained from $2n$ measurement functions ψ_k of the NtD map?

Now define $\beta_i = \int_{\partial\Omega} \zeta_i \, d\mathbf{x}$. The functions $\varphi_i \equiv \zeta_i / \beta_i \in H^{1/2}(\partial\Omega)$ meet all the requirements outlined in definition 1 to define a measured DtN map. In particular, they have disjoint supports and, by the duality relation (A.2) we have for $i \neq j$,

$$\begin{aligned} \langle \varphi_i, \Lambda_{1/\sigma}^{\text{DtN}} \varphi_j \rangle &= - \left\langle \varphi_i, \left(\frac{\partial}{\partial \theta} \Lambda_{\sigma}^{\text{NtD}} \frac{\partial}{\partial \theta} \right) \varphi_j \right\rangle = \left\langle \frac{\partial \varphi_i}{\partial \theta}, \Lambda_{\sigma}^{\text{NtD}} \frac{\partial \varphi_j}{\partial \theta} \right\rangle \\ &= \frac{1}{\beta_i \beta_j} \langle \psi_{2i} - \psi_{2i-1}, \Lambda_{\sigma}^{\text{NtD}} (\psi_{2j} - \psi_{2j-1}) \rangle. \end{aligned} \quad (\text{A.4})$$

Thus, by doing a numerical tangential derivative of the NtD data for σ , we can extract a measured DtN map for $1/\sigma$. We illustrate the process with figure A1. The matrix version of (A.4) is surprisingly simple:

$$\mathcal{M}_n(\Lambda_{1/\sigma}^{\text{DtN}}) = \mathcal{Z}(\mathbf{D}^T \mathcal{M}_{2n}(\Lambda_{\sigma}^{\text{NtD}}) \mathbf{D}), \quad (\text{A.5})$$

where $\mathcal{Z}(\mathbf{A}) := \mathbf{A} - \text{diag}(\mathbf{A}\mathbf{1})$ and $\mathbf{D} \in \mathbb{R}^{2n \times n}$ is the matrix given columnwise by

$$\mathbf{D} = [\beta_1(\mathbf{e}_1 - \mathbf{e}_2), \beta_2(\mathbf{e}_3 - \mathbf{e}_4), \dots, \beta_n(\mathbf{e}_{2n-1} - \mathbf{e}_{2n})].$$

Another immediate consequence of (A.4) is that we can formulate corollaries to the results we obtained in appendix C on the consistency of DtN map measurements with the resistor network model. Specifically, we can derive necessary conditions for the NtD map based on the necessary conditions of Ingerman and Morrow [32].

Appendix B. Numerical experiments supplement

B.1. Conductivity definitions

The conductivities used in our numerical experiments appear in figure 5. The precise definition of each conductivity follows.

Conductivity ‘sigX’ is depicted in figure 5 (left) and it is a smooth function given by the superposition of two Gaussian bell functions. Specifically,

$$\sigma(\mathbf{x}) = 1 + \frac{1}{2} \psi(\|\mathbf{x}\|_2) [\exp(-\|\mathbf{A}(\mathbf{x} - \mathbf{a})\|_2^2) + \exp(-\|\mathbf{B}(\mathbf{x} - \mathbf{b})\|_2^2)],$$

where $\mathbf{a} = (0.3, 0.3)^T$, $\mathbf{b} = (-0.4, -0.4)^T$ and the matrices \mathbf{A} and \mathbf{B} are,

$$\mathbf{A} = \mathbf{Q} \begin{bmatrix} \sqrt{20} & 0 \\ 0 & 1 \end{bmatrix} \mathbf{Q}^T, \quad \mathbf{B} = \mathbf{Q} \begin{bmatrix} 1 & 0 \\ 0 & \sqrt{20} \end{bmatrix} \mathbf{Q}^T, \quad \text{with } \mathbf{Q} = \frac{-1}{\sqrt{2}} \begin{bmatrix} 1 & 1 \\ 1 & -1 \end{bmatrix}.$$

The function $\psi(t)$ is a smooth cutoff function that ensures $\sigma|_{\partial\Omega} = 1$ by having $\psi(t) = 0$ for $t \geq 0.99$ and $\psi(t) = 1$ for $t \leq 0.5$. The smooth transition from 0 to 1 on $[0.5, 0.99]$ is obtained by an affine mapping of the function $\exp(1 + 1/s^2)$ defined on $[0, 1]$.

Conductivity ‘phantom1’ is depicted in figure 5 (right) and it is a piecewise constant function that represents a simplified chest phantom with conductivities relative to the background close

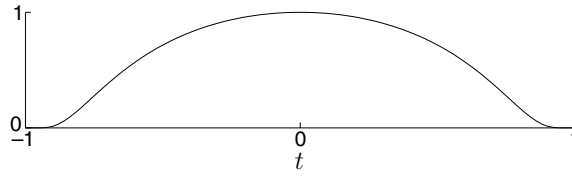


Figure B1. The smoothed box function $\varphi(t)$ we use to define the measured DtN map, rescaled to have values in $[0, 1]$.

to those of the human body during expiration [35, section 5.1]. The background conductivity is 1. The lungs are simulated by two ellipses with conductivity $1/3$ and the heart has conductivity 2.

B.2. A smoothed box function

We recall from section 3.1 that the measured DtN map $\mathcal{M}_n(\Lambda_\sigma)$ consists of measurements taken with n nonnegative functions φ_i defined on the boundary $\partial\Omega$ and that have disjoint supports. In the numerics, all φ_i are patterned from a single function and we explain here how this is done.

We parametrize the boundary $\partial\Omega$ by an angle $\theta \in [0, 2\pi]$, and by a slight abuse of notation $\varphi_i(\theta)$ represents $\varphi_i(\mathbf{x}(\theta))$. Then the functions φ_i are constructed from a single function $\varphi(t)$ with $\text{supp } \varphi \subset (-1, 1)$, by setting

$$\varphi_i(\theta) = (n/\pi)\varphi((n/\pi)(\theta - 2i\pi/n)).$$

This ensures the supports of φ_i are disjoint since $\text{supp } \varphi_i \subset 2i\pi/n + (-\pi/n, \pi/n)$.

We chose φ as the smoothed box function depicted in figure B1, rescaled so that $\int_{-1}^1 \varphi(t) dt = 1$. This function is such that $\varphi(t) = 1$ for $|t| \leq 0.1$ and $\varphi(t) = 0$ for $|t| \geq 0.9$. The smooth transition from 0 to 1 on $[0.1, 0.9]$ and $[-0.9, -0.1]$ is obtained by an affine mapping of the function $\exp(1 + 1/s^2)$ defined on $[0, 1]$.

Appendix C. Proof of theorem 1

We must show that the measurements $\mathcal{M}_n(\Lambda_\sigma^{\text{DtN}})$ belong to \mathcal{D}_n , the set of DtN maps of well-connected resistor networks. This set is defined in [20] as follows.

Definition 3. \mathcal{D}_n is the set of matrices $\mathbf{A} \in \mathbb{R}^{n \times n}$ such that

- (i) The matrix \mathbf{A} is symmetric.
- (ii) The matrix \mathbf{A} has zero row sum, i.e. $\mathbf{A}\mathbf{1} = \mathbf{0}$.
- (iii) All circular minors \mathbf{M} of \mathbf{A} are totally negative, i.e. $\det(-\mathbf{M}) > 0$. A circular minor of \mathbf{A} is a submatrix $\mathbf{M} = \mathbf{A}(p_1, \dots, p_k; q_1, \dots, q_k)$, with distinct indices p_i and q_i between 1 and n , for $1 \leq i \leq k$. The indices are sorted so that points $v_{p_1}, \dots, v_{p_k}, v_{q_k}, \dots, v_{q_1}$ appear in order on $\partial\Omega$.

That $\mathcal{M}_n(\Lambda_\sigma^{\text{DtN}})$ is a symmetric $n \times n$ matrix, with zero row sum, follows trivially from definition 1 and the self-adjointness of $\Lambda_\sigma^{\text{DtN}}$. The technical part is to show that all the circular minors of $\mathcal{M}_n(\Lambda_\sigma^{\text{DtN}})$ are totally negative (see e.g. [20, section 10] for a definition).

To establish the total negativity of the circular minors of the measured DtN map, we use a characterization of the kernel of the DtN map due to Ingerman and Morrow [32]. Recall that the kernel $K_\sigma : \partial\Omega \times \partial\Omega \rightarrow \mathbb{R}$ of the DtN map is such that for $f \in H^{1/2}(\partial\Omega)$,

$$(\Lambda_\sigma^{\text{DtN}} f)(\mathbf{x}) = \int_{\partial\Omega} K_\sigma(\mathbf{x}, \mathbf{y}) f(\mathbf{y}) \, d\mathbf{y}.$$

We require some terminology to review the results in [32].

Definition 4. A set of $2k$ distinct points $\{\mathbf{x}_1, \dots, \mathbf{x}_k, \mathbf{y}_1, \dots, \mathbf{y}_k\}$ of $\partial\Omega$ is called a circular pair if $\mathbf{x}_1, \dots, \mathbf{x}_k, \mathbf{y}_k, \dots, \mathbf{y}_1$ are consecutive on the circle. Similarly, a set of $2k$ nonnegative functions $\{X_1, \dots, X_k, Y_1, \dots, Y_k\}$, with supports $I_1, \dots, I_k, J_1, \dots, J_k$ in $\partial\Omega$, is called a circular pair of functions if their supports are disjoint and are consecutive on the circle when numbered $I_1, \dots, I_k, J_k, \dots, J_1$. Additionally, each function should integrate to one.

Definition 5. A kernel $K : \partial\Omega \times \partial\Omega \rightarrow \mathbb{R}$ is said to have property **(P1)** if and only if, for all circular pairs $\{\mathbf{x}_1, \dots, \mathbf{x}_k, \mathbf{y}_1, \dots, \mathbf{y}_k\}$, and for all integers k , the following determinantal inequality holds

$$\det(\{-K(\mathbf{x}_i, \mathbf{y}_j)\}_{i,j=1,\dots,k}) > 0. \quad (\text{C.1})$$

Note that it is possible to take pointwise evaluations of the kernel $K_\sigma(\mathbf{x}, \mathbf{y})$ when it is continuous away from the diagonal $\mathbf{x} = \mathbf{y}$. This holds for example for C^2 conductivities (see [32]).

Definition 6. A kernel $K : \partial\Omega \times \partial\Omega \rightarrow \mathbb{R}$ is said to have property **(P2)** if and only if, for all circular pairs of functions $\{X_1, \dots, X_k, Y_1, \dots, Y_k\}$, and for all integers k , the following determinantal inequality holds

$$\det\left(\left\{-\int_{\partial\Omega \times \partial\Omega} X_i(\mathbf{x}) Y_j(\mathbf{y}) K(\mathbf{x}, \mathbf{y}) \, d\mathbf{x} \, d\mathbf{y}\right\}_{i,j=1,\dots,k}\right) > 0. \quad (\text{C.2})$$

It is clear from definition 1 that to show the total negativity of the circular minors of $\mathcal{M}_n(\Lambda_\sigma^{\text{DtN}})$, it suffices to show that the kernel of the DtN map satisfies **(P2)**. The main result in [32] is that the kernel K_σ of the DtN map for a conductivity $\sigma \in C^2(\Omega)$ satisfies **(P1)**. We extended this result to more general measurements, by showing the equivalence between **(P1)** and **(P2)**, which is stated in the next theorem.

Theorem 3. Let $K : \partial\Omega \times \partial\Omega \rightarrow \mathbb{R}$ be a kernel, continuous away from the diagonal, and such that $\lim_{\mathbf{y} \rightarrow \mathbf{x}} K(\mathbf{x}, \mathbf{y}) = -\infty$. Then **(P1)** holds for K iff **(P2)** holds for K .

In order to prove theorem 3, let us show first an intermediary lemma, involving the weaker properties **(WP1)** and **(WP2)**, which are obtained by replacing the strict inequalities in definitions 5 and 6, by non-strict inequalities. Note that the assumptions on K in the lemma are relaxed, compared to those of theorem 3. The singularity of the kernel on the diagonal is not required.

Lemma 2. Let $K : \partial\Omega \times \partial\Omega \rightarrow \mathbb{R}$ be some continuous kernel away from the diagonal. Then **(WP1)** holds for K if and only if **(WP2)** holds for K .

Proof. We use the techniques of lemma 6.1 in [32]. Let K be a kernel satisfying the assumptions of the theorem. Let us start by assuming **(WP1)** holds. If $\{X_1, \dots, X_k, Y_1, \dots, Y_k\}$ is some

circular pair of functions, using the combinatorial definition of the determinant, and reducing the domain of integration to the support of the functions involved, we may write,

$$\det \left(\left\{ - \int_{I_i \times J_j} X_i(\mathbf{x}) Y_j(\mathbf{y}) K(\mathbf{x}, \mathbf{y}) \, d\mathbf{x} \, d\mathbf{y} \right\}_{i,j=1,\dots,k} \right) = \sum_{\tau \in \Pi(1,\dots,k)} \text{sgn}(\tau) \prod_{i=1}^k \left(- \int_{I_i \times J_{\tau(i)}} X_i(\mathbf{x}_i) Y_{\tau(i)}(\mathbf{y}_{\tau(i)}) K(\mathbf{x}_i, \mathbf{y}_{\tau(i)}) \, d\mathbf{x}_i \, d\mathbf{y}_{\tau(i)} \right), \quad (\text{C.3})$$

where $\Pi(1, \dots, k)$ is the set of all $k!$ permutations of $1, \dots, k$, and the sign of a permutation τ is defined by

$$\text{sgn}(\tau) = \begin{cases} +1 & \text{if } \tau \text{ is equivalent to an even number of transpositions,} \\ -1 & \text{if } \tau \text{ is equivalent to an odd number of transpositions.} \end{cases}$$

Now, we obtain after some reordering,

$$\sum_{\tau \in \Pi(1,\dots,k)} \text{sgn}(\tau) \int_{I_1 \times J_1} \cdots \int_{I_k \times J_k} d\mathbf{x}_1 \, d\mathbf{y}_1 \cdots d\mathbf{x}_k \, d\mathbf{y}_k \left(\prod_{i=1}^k -K(\mathbf{x}_i, \mathbf{y}_{\tau(i)}) \right) \left(\prod_{i=1}^k X_i(\mathbf{x}_i) Y_i(\mathbf{y}_i) \right)$$

and, identifying a determinant, we get

$$\det \left(\left\{ - \int_{I_i \times J_j} X_i(\mathbf{x}) Y_j(\mathbf{y}) K(\mathbf{x}, \mathbf{y}) \, d\mathbf{x} \, d\mathbf{y} \right\}_{i,j=1,\dots,k} \right) = \int_{I_1 \times J_1} \cdots \int_{I_k \times J_k} \times \det(\{-K(\mathbf{x}_i, \mathbf{y}_j)\}_{i,j=1,\dots,k}) \left(\prod_{i=1}^k X_i(\mathbf{x}_i) Y_i(\mathbf{y}_i) \right) d\mathbf{x}_1 \, d\mathbf{y}_1 \cdots d\mathbf{x}_k \, d\mathbf{y}_k. \quad (\text{C.4})$$

Note that $\{\mathbf{x}_1, \dots, \mathbf{x}_k, \mathbf{y}_1, \dots, \mathbf{y}_k\}$ is a circular pair of points, because $\mathbf{x}_i \in I_i, \mathbf{y}_i \in J_i$ and $I_1, \dots, I_k, J_k, \dots, J_1$ do not intersect, and they are consecutive when laid on a circle. Since K satisfies **(WP1)**, the determinant in the integrand is nonnegative, and so is the integrand itself, which proves **(WP1)** \Rightarrow **(WP2)**.

To prove **(WP2)** \Rightarrow **(WP1)**, construct a sequence of circular pairs of functions $\{X_1^{(p)}, \dots, X_k^{(p)}, Y_1^{(p)}, \dots, Y_k^{(p)}\}$ such that for $i, j = 1, \dots, k$, we have

$$\lim_{p \rightarrow \infty} \int_{\partial\Omega \times \partial\Omega} X_i^{(p)}(\mathbf{x}) Y_j^{(p)}(\mathbf{y}) K(\mathbf{x}, \mathbf{y}) \, d\mathbf{x} \, d\mathbf{y} = K(\mathbf{x}_i, \mathbf{y}_j).$$

Then **(WP1)** follows from the continuity of the determinant. \square

We can now write a proof of theorem 3, which follows essentially from [32].

Proof of theorem 3. Using (C.4) and strict inequalities in the argument for **(WP1)** \Rightarrow **(WP2)** in lemma 2, it follows that **(P1)** \Rightarrow **(P2)**. Assume then that **(P2)** holds for K , therefore **(WP2)** and by lemma 2 **(WP1)** hold for K , as well. Moreover Ingerman and Morrow [32, section 4], proved that provided K is a kernel continuous away from the diagonal and singular on the diagonal, we have **(WP1)** \Rightarrow **(P1)**. This completes the proof. \square

Remark 4. In the proof we assume complete knowledge of the DtN map. When we have measurements of this map at only N points on $\partial\Omega$, we can estimate the quadratic forms in $\mathcal{M}_n(\Lambda_\sigma^{\text{DtN}})$ using some quadrature rule. Then an analogous characterization holds [31, B.4]: there is a unique resistor network of type $C(l, n)$ that fits the measurements. Therefore we can use our algorithm unchanged when we have N measurements on $\partial\Omega$.

References

- [1] Alessandrini G 1988 Stable determination of conductivity by boundary measurements *Appl. Anal.* **27** 153–72
- [2] Allers A and Santosa F 1991 Stability and resolution analysis of a linearized problem in electrical impedance tomography *Inverse Problems* **7** 515–33
- [3] Astala K, Päiväranta L and Lassas M 2005 Calderón’s inverse problem for anisotropic conductivity in the plane *Commun. Partial Diff. Eqns* **30** 207–24
- [4] Ben Ameer H, Chavent G and Jaffré J 2002 Refinement and coarsening indicators for adaptive parametrization: application to the estimation of hydraulic transmissivities *Inverse Problems* **18** 775–94
- [5] Ben Ameer H and Kaltenbacher B 2002 Regularization of parameter estimation by adaptive discretization using refinement and coarsening indicators *J. Inverse Ill-Posed Problems* **10** 561–83
- [6] Borcea L 2002 Electrical impedance tomography *Inverse Problems* **18** R99–136 (topical review)
- [7] Borcea L, Berryman J G and Papanicolaou G C 1996 High-contrast impedance tomography *Inverse Problems* **12** 835–58
- [8] Borcea L, Berryman J G and Papanicolaou G C 1999 Matching pursuit for imaging high-contrast conductivity *Inverse Problems* **15** 811–49
- [9] Borcea L and Druskin V 2002 Optimal finite difference grids for direct and inverse Sturm–Liouville problems *Inverse Problems* **18** 979–1001
- [10] Borcea L, Druskin V and Knizhnerman L 2005 On the continuum limit of a discrete inverse spectral problem on optimal finite difference grids *Commun. Pure Appl. Math.* **58** 1231–79
- [11] Borcea L, Druskin V and Mamonov A 2007 Solving the discrete EIT problem with optimization techniques *Schlumberger-Doll Report*
- [12] Borsic A 2002 Regularisation methods for imaging from electrical measurements *PhD Thesis* Oxford Brookes University
- [13] Borsic A, Graham B M, Adler A and Lionheart W R 2007 Total variation regularization in electrical impedance tomography *Technical Report 92* School of Mathematics, University of Manchester
- [14] Calderón A-P 1980 On an inverse boundary value problem *Seminar on Numerical Analysis and its Applications to Continuum Physics (Rio de Janeiro, 1980)* (Rio de Janeiro: Soc. Brasil. Mat.) pp 65–73
- [15] Cheney M, Isaacson D, Newell J, Simske S and Goble J 1990 Noser: an algorithm for solving the inverse conductivity problem *Int. J. Imaging Syst. Technol.* **2** 66–75
- [16] Cherkaeva E and Tripp A C 1996 Inverse conductivity problem for inaccurate measurements *Inverse Problems* **12** 869–83
- [17] Colin de Verdière Y 1994 Réseaux électriques planaires: I *Comment. Math. Helv.* **69** 351–74
- [18] Colin de Verdière Y, Gitler I and Vertigan D 1996 Réseaux électriques planaires: II *Comment. Math. Helv.* **71** 144–67
- [19] Curtis E, Mooers E and Morrow J 1994 Finding the conductors in circular networks from boundary measurements. *RAIRO Modél. Math. Anal. Numer.* **28** 781–814
- [20] Curtis E B, Ingerman D and Morrow J A 1998 Circular planar graphs and resistor networks *Linear Algebra Appl.* **283** 115–50
- [21] Curtis E B and Morrow J A 2000 *Inverse Problems for Electrical Networks (Series on Applied Mathematics vol 13)* (Singapore: World Scientific)
- [22] Daubechies I, Defrise M and De Mol C 2004 An iterative thresholding algorithm for linear inverse problems with a sparsity constraint *Commun. Pure Appl. Math.* **57** 1413–57
- [23] Deuffhard P 2004 *Newton Methods for Nonlinear Problems. Affine Invariance and Adaptive Algorithms (Springer Series in Computational Mathematics vol 35)* (Berlin: Springer)
- [24] Dines K A and Lytle R J 1981 Analysis of electrical conductivity imaging *Geophysics* **46** 1025–36
- [25] Dobson D C 1990 Stability and regularity of an inverse elliptic boundary value problem *PhD Thesis* Rice University (Technical Report TR90-14)
- [26] Dobson D C 1992 Convergence of a reconstruction method for the inverse conductivity problem *SIAM J. Appl. Math.* **52** 442–58
- [27] Dobson D C and Santosa F 1994 An image-enhancement technique for electrical impedance tomography *Inverse Problems* **10** 317–34
- [28] Druskin V 1982 The unique solution of the inverse problem of electrical surveying and electrical well-logging for piecewise-continuous conductivity *Izv. Earth Phys.* **18** 51–3
- [29] Engl H W, Hanke M and Neubauer A 1996 *Regularization of Inverse Problems* (Dordrecht: Kluwer)
- [30] Gisser D G, Isaacson D and Newell J C 1990 Electric current computed tomography and eigenvalues *SIAM J. Appl. Math.* **50** 1623–34
- [31] Guevara Vasquez F 2006 On the parametrization of ill-posed inverse problems arising from elliptic partial

- differential equations *Technical Report TR-06-13* Computational and Applied Mathematics Department, Rice University, Houston, TX
- [32] Ingerman D and Morrow J A 1998 On a characterization of the kernel of the Dirichlet-to-Neumann map for a planar region *SIAM J. Math. Anal.* **29** 106–15 (electronic)
 - [33] Ingerman D V 2000 Discrete and continuous Dirichlet-to-Neumann maps in the layered case *SIAM J. Math. Anal.* **31** 1214–34 (electronic)
 - [34] Isaacson D 1986 Distinguishability of conductivities by electric current computed tomography *IEEE Trans. Med. Imaging* **MI-5** 91–5
 - [35] Knudsen K, Mueller J and Siltanen S 2004 Numerical solution method for the dbar-equation in the plane *J. Comput. Phys.* **198** 500–17
 - [36] Kohn R and Vogelius M 1984 Determining conductivity by boundary measurements *Commun. Pure Appl. Math.* **37** 289–98
 - [37] Kolehmainen V 2001 Novel approaches to image reconstruction in diffusion tomography *PhD Thesis* Kuopio University
 - [38] MacMillan H R, Manteuffel T A and McCormick S F 2004 First-order system least squares and electrical impedance tomography: part II. Unpublished manuscript
 - [39] Mandache N 2001 Exponential instability in an inverse problem for the Schrödinger equation *Inverse Problems* **17** 1435–44
 - [40] Nachman A I 1996 Global uniqueness for a two-dimensional inverse boundary value problem *Ann. Math.* (2) **143** 71–96
 - [41] Nocedal J and Wright S J 1999 *Numerical Optimization (Operations Research)* (New York: Springer)
 - [42] Seagar A 1983 Probing with low frequency electric currents *PhD Thesis* University of Canterbury, UK
 - [43] Somersalo E, Cheney M and Isaacson D 1992 Existence and uniqueness for electrode models for electric current computed tomography *SIAM J. Appl. Math.* **52** 1023–40
 - [44] Somersalo E, Cheney M, Isaacson D and Isaacson E 1991 Layer stripping: a direct numerical method for impedance imaging *Inverse Problems* **7** 899–926
 - [45] Sylvester J and Uhlmann G 1987 A global uniqueness theorem for an inverse boundary value problem *Ann. Math.* (2) **125** 153–69
 - [46] Uhlmann G 1999 Developments in inverse problems since Calderón’s foundational paper *Harmonic Analysis and Partial Differential Equations (Chicago, IL, 1996) (Chicago Lectures in Math.)* (Chicago, IL: University Chicago Press) pp 295–345
 - [47] Vogel C R 2002 *Computational Methods for Inverse Problems (Frontiers in Applied Mathematics)* (Philadelphia: SIAM)